ERDC/CERL TR-02-1

US Army Corps of Engineers®
Engineer Research and Development Center

Evaluating Strength and Stiffness of Unreinforced Masonry Infill Structures

Ghassan Al-Chaar

January 2002

Construction Engineering Research Laboratory

Foreword

This study was conducted for Headquarters, U.S. Army Corps of Engineers, under project 622784AT41, "Military Facilities Engineering Technologies (6.2 Exploratory Development)," PROMIS No. CFM-A011, "Seismic Rehabilitation of Concrete Frames with Infill." The technical monitor was David C. Bohl, CECW-EW.

The work was performed by the Materials and Structures Branch (CF-M) of the Facilities Division (CF), Construction Engineering Research Laboratory (CERL). The CERL Principal Investigator was Dr. Ghassan Al-Chaar. The technical editor was Linda L. Wheatley, Information Technology Laboratory — Champaign. Martin J. Savoie is Chief, CF-M, and L. Michael Golish is Chief, CF. The associated Technical Director was Dr. Paul A. Howdyshell. The Director of CERL is Dr. Alan W. Moore. The author wishes to thank Dr. Dan P. Abrams for his review and input for this research project, Dr. Richard Klingler and Dr. Mohsen Issa for their input, and Greg Lamb and Dr. Richard Angel for their assistance in developing the document. The COE Seismic Review Panelists: Joseph P. Hartman, HQ02, Ghassem Khosrownia, SPK, Thomas D. Wright, NWK, and David C. Bohl, HQ02, provided technical guidelines for the project. Thanks also go to the Seismic and Structural Engineering team members Dr. John R. Hayes, Jr. and Steven C. Sweeney for their review and input.

CERL is an element of the Engineer Research and Development Center (ERDC), U.S. Army Corps of Engineers. The Commander and Executive Director of ERDC is COL John W. Morris III, EN, and the Director of ERDC is Dr. James R. Houston.

Contents

List of Figures and Tables

Figures

Tables

1 Introduction

Background

Masonry is one of the oldest construction materials currently in use around the world for reasons that include accessibility, functionality, and cost. This material has been used for hundreds of years in construction projects ranging from simple roadways to complex arch designs. Masonry has also commonly been used in frame building structures as infill, where it was intended to act as an environmental divider rather than a structural element. The primary function of masonry was either to protect the inside of the structure from the environment (rain, snow, wind, etc.) or to divide inside spaces. In either case, common practice has always been to ignore infill during the design and analysis of steel/reinforced concrete frame structures.

Contrary to common practice, the presence of masonry infills influence the overall behavior of structures when subjected to lateral forces. When masonry infills are considered to interact with their surrounding frames, the lateral stiffness and the lateral load capacity of the structure largely increase.

Extensive research has been done during the last 50 years to determine how the presence of masonry infills influences the in-plane and the out-of-plane behavior of steel/reinforced concrete frame structures (building types 7 or 10 as classified by the Federal Emergency Management Agency (FEMA) in Table 1. Experimental research on specimens ranging from full size to 1:8 scale with varying numbers of bays and stories, in addition to analytical work ranging from simple mechanics to complex nonlinear finite element analyses, have yielded great insight into infill-frame interaction and behavior.

The influence of infills on overall behavior of the structure has been found to change with the direction in which the load is applied. This report gives guidelines on evaluating the lateral load capacity of infilled panels for in-plane and out-of-plane loading. Further, guidelines are given that account for the effect of out-of-plane loading on in-plane capacity.

Table 1. FEMA building categories.

Type	Building Description
1	Wood Light Frames
2	Wood Frames, Commercial and Industrial
3	Steel Moment Frames
4	Steel Braced Frames
5	Steel Light Frames
6	Steel Frames with Concrete Shear Walls
7	Steel Frames with Infill Masonry Shear Walls
8	Concrete Moment Frames
9	Concrete Shear Wall Buildings
10	Concrete Frames with Infill Masonry Shear Walls
11	Precast/Tile-up Concrete Shear Wall Buildings
12	Precast Concrete Frames
13	Reinforced Masonry Bearing Wall Buildings with Flexible Diaphragms
14	Reinforced Masonry Bearing Wall Buildings with Stiff Diaphragms
15	Unreinforced Masonry Bearing Wall Buildings

Objective

The objective of this research was to provide guidelines for evaluating strength and stiffness of unreinforced masonry (URM) infill panels in military structures subjected to lateral forces. The guidelines are based on experimental and computational research performed at the U.S. Army Engineer Research and Development Center (ERDC) and include a number of empirically based relationships for estimating strength and stiffness of infill panels subjected to forces applied either normal to or parallel with their plane. These guidelines should prove useful for engineering evaluations of the lateral strength of building structures with respect to wind or earthquake forces. The guidelines give the engineer a strength-based alternative to FEMA 273, a performance-based method, which should also result in safe and economical construction.

Approach

The information compiled in this report was written following a logical sequence intended to help the engineer in the evaluation process. First, the following chapter outlines the steps that must be followed to obtain all the required material and geometrical properties of the structure to be evaluated. In the next chapters, the in-plane strength and stiffness evaluation procedures are presented for the infill-frame lateral-force resisting system. Then, the out-of-plane strength and stiffness evaluation method is presented, along with the effects of

out-of-plane loading on in-plane capacity. The final chapter proposes alternative analysis methods for engineers unable to use the nonlinear static analysis presented in this report. Appendix A includes an illustrative example to help summarize and clarify the entire evaluation process, and Appendix B is a commentary on selected sections of the evaluation.

Scope

The evaluation procedures presented in this document (based on life-safety performance) are applicable to all building structures that have been constructed using either steel or reinforced concrete frames, and walls that consist of infill panels constructed of solid clay brick, concrete block, and hollow clay tile masonry. These types of structures correspond to Building Types 7 and 10 as defined in Chapter 2 and in accordance with FEMA 310.

Mode of Technology Transfer

This report is to be used as a complement to applicable provisions in FEMA 310 with respect to seismic evaluation of buildings.

This report will be made accessible through the World Wide Web (WWW) at URL: http://www.cecer.army.mil

Units of Weight and Measure

U.S. standard units of measure are used throughout this report. A table of conversion factors for Standard International (SI) units is provided below.

SI conversion factors		
1 in.	=	2.54 cm
1 sq in.	=	6.452 cm^2
1 lb	=	0.453 kg
1 kip	=	453 kg
1 psi	=	6.89 kPa

2 General Requirements

FEMA classifies all building structures into 15 categories depending on the type of lateral resisting system of the structure as presented in Table 1. This report covers only the evaluation of infill panels considered as structural components of buildings in categories 7 and 10.

Geometrical and Mechanical Properties

Strength assessment for these types of structures requires the recollection of all related specimen geometrical and mechanical properties. All geometrical properties, including the size and location of all masonry infills and all confining frame elements, should be determined. Infill dimensions such as height (h), length (l), and thickness (t) should be obtained from field measurements or existing construction/structural plans. All relevant dimensions for the frame elements must also be obtained (H, L_f, h_b, b_b, h_c, b_c, etc.). Definitions of these dimensions are given in the glossary.

Tests required to evaluate mechanical material properties of the masonry infills such as compressive strength (f'_m), modulus of elasticity in compression (E_m), and shear strength (f'_v) must be carried out in accordance with Section 7.3.2 (Properties of In-Place materials) of FEMA 273. Evaluation of material properties for the confining frame should be executed in accordance with either Section 6.3.2 (for reinforced concrete frames) or Section 5.3.2 (for steel frames) of FEMA 273. Material properties can also be obtained from building codes from the year of construction of the building being evaluated, or from as-built plans if available.

Masonry Infill Panels

Masonry infill panels should be evaluated in both the in-plane and out-of-plane direction while accounting for the effects of out-of-plane loading on in-plane capacity. In general, infills can be grouped into two different categories: isolated infills and “regular” infills (sometimes referred to as shear infills).

Isolated infills are panels totally isolated from the confining frame at the top and on both sides. The isolation (gaps) between the infill and the frame must be greater than any possible deformation expected by the frame, thus prohibiting any infill/frame interaction. These infills are not considered structural elements.

This report focuses on the second category, "regular" infills, where the panels act as part of the lateral force-resisting system of the structure. An infill in this category must be fully in tight contact with its confining frame on all four of its sides. Any gaps must be completely filled to guarantee full mortar bonding contact.

In-plane and out-of-plane behavior of infilled frames depends on a number of factors outside of the basic mechanical and geometrical properties of the infill and frame. These additional factors alter the original stiffness and strength of infilled frames. The empirically developed factors presented in this report modify original infilled frame performance estimates by taking into account existing infill damage, flexibility of confining frame elements, and presence of infill openings. These multiplicative factors will be discussed in later sections.

3 In-Plane Strength Evaluation of URM Infills

Background

The transfer of lateral forces across infilled frames causes nonuniform stress distribution within the infill and frame elements. As the lateral forces are increased, the stress distribution varies until failure of the infill occurs. Failure of the infill occurs when either its shear or compressive strength is reached.

The expected flexural and shear strength of the frame elements confining the infill panel must also be evaluated. Column and beam shear and flexural strengths must exceed the horizontal/vertical components of the force required for failure of the infill. This procedure assures failure of the infill before failure in the confining frame occurs.

The lateral load capacity of frame-infill systems should be found using a nonlinear finite element program which captures the nonlinear behavior of all material components: masonry, mortar, concrete, and steel. Because this option is not available or is impractical in most situations, however, a simpler analytical method is proposed. The proposed method is a pushover analysis of a frame containing eccentric equivalent struts that represent the masonry. The method can be used for fully infilled frames as well as partially infilled and perforated masonry panels. Using eccentric struts in this global analysis will yield infill effects on the column directly, which will negate the need to evaluate these members locally. This method relies on the development of plastic hinges to capture the nonlinearities of the structural system. The proposed method has been proven to give reliable results based on experimental data and nonlinear finite element analysis. The following section gives a general outline of the process of performing a pushover analysis on an infilled frame.

General Procedure for Evaluating the Capacity of Infilled Frames Using Pushover Analyses

The following procedure is a general outline of what is required by standard structural analysis programs in order to perform a pushover analysis. More or less information may be required for a specific program.

1. Draw Frame Elements with the geometry, restraints, and material properties found in the existing structure. In general, the required material properties consist of f'_c, f_y, E_c, and E_s. Definitions of these properties are given in the glossary.
2. Draw Equivalent Struts representing the infilled panels and place them eccentrically with respect to the columns. This eccentric distance is referred to as l_{column} and is defined by Equation 4*. The strut thickness should be the same as the net thickness of the infill material it represents. The width of the equivalent strut, a, should be calculated using Equation 2. If the infilled panel is either partially infilled or perforated, the modifications in sections on partially infilled frames and perforated panels (p 20), respectively, must be applied. Furthermore, existing infill damage must be taken into account by following the corresponding section on page 21. The material properties that should be assigned to the strut consist of R_{strut} and E_m, where R_{strut} is the capacity of the strut and is computed using Equation 7.
3. Assign Plastic Hinges to frame members with the load-deformation behavior appropriate for the particular structural section and material. For beams, the plastic hinge should identify nonlinear behavior for flexure and shear. For columns, the hinge should account for the interaction between axial load and flexure as well as capture the nonlinearities associated with shearing. The hinge properties may be calculated using the guidelines given in Section 6.4 of FEMA 273 for reinforced concrete members or Section 5.4 for steel members. The hinges in the columns should be located at a minimum distance l_{column} from the face of the beam, while hinges in the beam should be located at a minimum distance l_{beam} from the face of the column.
4. Assign Plastic Hinges to the midspan of the Eccentric Equivalent Struts. The load-deformation characteristics should be consistent with Figure 9 (p 23).
5. Assign Rigid End Offsets (REOs) to the joints of the frame in order to represent the decreased flexibility of the frame members confined by infill. The REOs

* Equations referenced in this section are shown beginning on page 18 of the next section.

should extend from the joint outward along the beams and columns until a plastic hinge is intersected.

6. Apply the gravity loads as initial conditions of the pushover analysis. The load combinations recommended are those found in Equations 3-2 and 3-3 in FEMA 273. The lateral loads should be applied in a manner that approximates the inertia forces in the design earthquake. The recommended inertia force distributions are given in Section 3.3.3.2 of FEMA 273.
7. Perform the Pushover Analysis using any member-unloading method to obtain equilibrium after a plastic hinge loses capacity due to excessive deformation.

Using the general procedure outlined above, an engineer can reasonably predict the in-plane capacity of infilled frames. The following sections describe the evaluation process in more detail.

Equivalent Strut Width

In-plane strength predictions of infilled frames are a complex, statically indeterminate problem. The strength of a composite-infilled frame system is not simply the summation of the infill properties plus those of the frame. Great efforts have been invested, both analytically and experimentally, to better understand and estimate the composite behavior of masonry-infilled frames. Polyakov (1960) (work dating back to the early 1950s), Stafford-Smith (1962, 1966, 1969), Mainstone (1971), Klingner and Bertero (1976, 1978), to mention just a few, formed the basis for understanding and predicting infilled frame in-plane behavior. Their experimental testing of infilled frames under lateral loads resulted in specimen deformation shapes similar to the one illustrated in Figure 1.

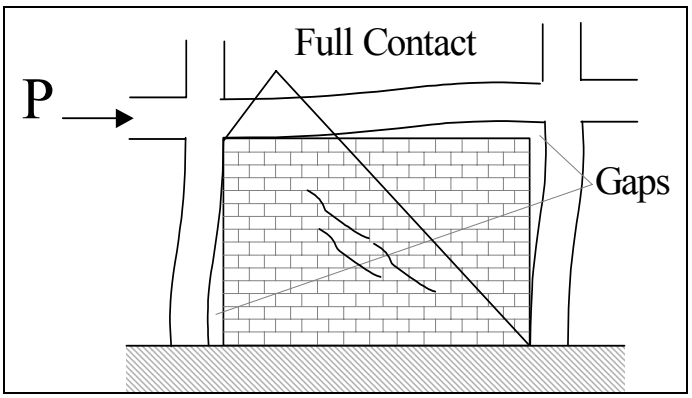

Figure 1. Specimen deformation shape.

During testing of the specimens, diagonal cracks developed in the center of the panel, and gaps formed between the frame and the infill in the nonloaded diagonal corners of the specimens, while full contact was observed in the two loaded diagonal corners. This behavior, initially observed by Polyakov, lead to a simplification in infilled frame analysis by replacing the masonry infill with an equivalent compressive masonry strut as shown in Figure 2.

The equivalent masonry strut of width, a, with same net thickness and mechanical properties (such as the modulus of elasticity E_m) as the infill itself, is assumed to be pinned at both ends to the confining frame.

The evaluation of the equivalent width, a, varies from one reference to the other. The most simplistic approaches presented by Paulay and Priestley (1992) and Angel et al. (1994) have assumed constant values for the strut width, a, between 12.5 to 25 percent of the diagonal dimension of the infill, with no regard for any infill or frame properties. Stafford-Smith and Carter (1969), Mainstone (1971), and others, derived complex expressions to estimate the equivalent strut width, a, that consider parameters like the length of contact between the column/beam and the infill, as well as the relative stiffness of the infill to the frame.

The expressions used in this report have been adopted from Mainstone (1971) and Stafford-Smith and Carter (1969) for their consistently accurate predictions of infilled frame in-plane behavior when compared with experimental results (Mainstone 1971; Stafford-Smith and Carter 1969; Klingner and Bertero 1978; and Al-Chaar 1998).

The masonry infill panel will be represented by an equivalent diagonal strut of width, a, and net thickness t_{eff} as shown in Figure 3.

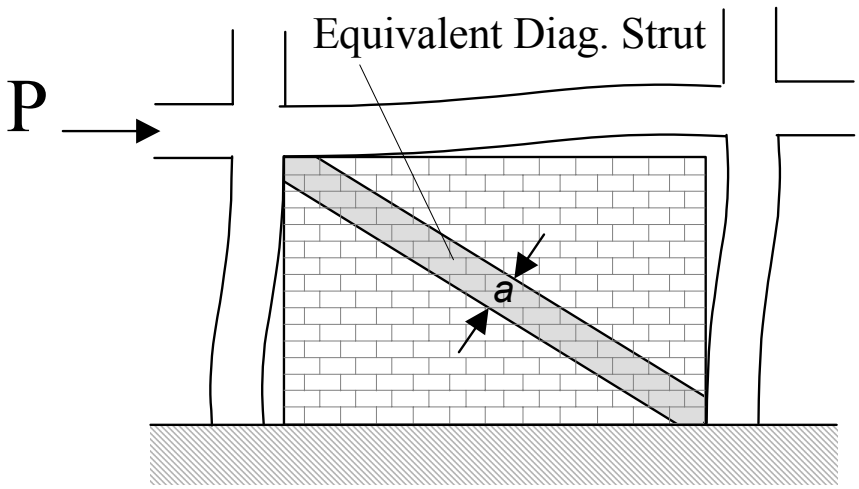

Figure 2. Equivalent diagonal strut.

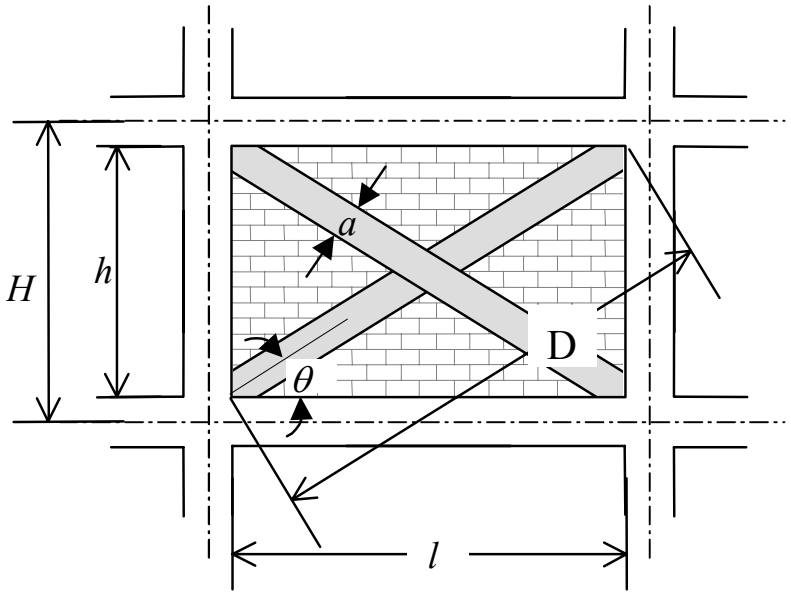

Figure 3. Strut geometry.

The equivalent strut width, a, depends on the relative flexural stiffness of the infill to that of the columns of the confining frame. The relative infill to frame stiffness shall be evaluated using Equation 1 (Stafford-Smith and Carter 1969):

$$\lambda_1 H \quad H \left(\frac{E_m t \sin 2\theta}{4 E_c I_{col} h} \right)^{1/4} \qquad \textbf{[Eq 1]}$$

Using this expression, Mainstone (1971) considers the relative infill to frame flexibility in the evaluation of the equivalent strut width of the panel as shown in Equation 2.

$$a \quad 0.175 D (\lambda_1 H)^{-0.4} \qquad \textbf{[Eq 2]}$$

However, if there are openings present and/or existing infill damage, the equivalent strut width must be reduced using Equation 3.

$$a_{red} = a (R_1)_i (R_2)_i \qquad \textbf{[Eq 3]}$$

Where:

$(R_1)_i$ = reduction factor for in-plane evaluation due to presence of opening defined in the section on perforated panels (p 20).

$(R_2)_i$ = reduction factor for in-plane evaluation due to existing infill damage defined in the corresponding section on page 21.

Although the expression for equivalent strut width given by Equation 2 was derived to represent the elastic stiffness of an infill panel, this document will extend its use to determine the ultimate capacity of infilled structures. The strut will be assigned strength parameters consistent with the properties of the infill it represents. A nonlinear static procedure, commonly referred to as a pushover analysis, will be used to determine the capacity of the infilled structure.

Eccentricity of Equivalent Strut

The equivalent masonry strut is to be connected to the frame members as depicted in Figure 4. The infill forces are assumed to be mainly resisted by the columns, and the struts are placed accordingly. The strut should be pin-connected to the column at a distance l_{column} from the face of the beam. This distance is defined in Equations 4 and 5 and is calculated using the strut width, a, without any reduction factors.

$$l_{column} = \frac{a}{\cos \theta_{column}} \quad \textbf{[Eq 4]}$$

$$\tan \theta_{column} = \frac{h - \dfrac{a}{\cos \theta_{column}}}{l} \quad \textbf{[Eq 5]}$$

Using this convention, the strut force is applied directly to the column at the edge of its equivalent strut width, a. This concept is illustrated in Figure 4.

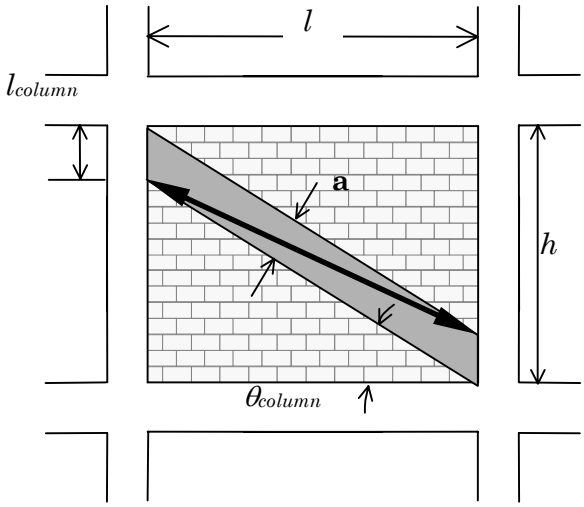

Figure 4. Placement of strut.

Partially Infilled Frames

In the case of a partially infilled frame, the reduced column length, l_{column}, shall be equal to the unbraced opening length for the windward column, while l_{column} for the leeward column is defined as usual (Figure 5). The strut width should be calculated from Equation 3, using the reduced infill height for h in Equation 1. Furthermore, the only reduction factor that should be taken into account is $(R_2)_i$, which accounts for existing infill damage.

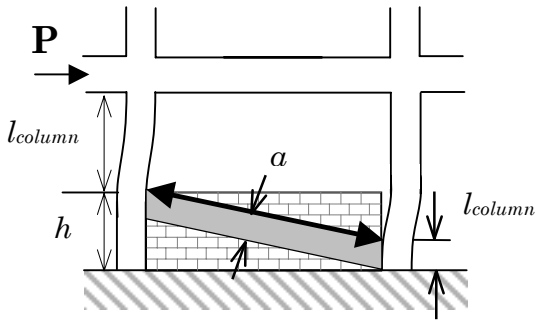

Figure 5. Partially infilled frame.

Perforated Panels

In the case of a perforated masonry panel, the equivalent strut is assumed to act in the same manner as for the fully infilled frame. Therefore, the eccentric strut should be placed at a distance l_{column} from the face of the beam as shown in Figure 6. The equivalent strut width, a, shall be multiplied, however, by a reduction factor to account for the loss in strength due to the opening. The reduction factor, $(R_1)_i$, is calculated using Equation 6.

$$(R_1)_i \quad 0.6\left(\frac{A_{open}}{A_{panel}}\right)^2 \quad 1.6\left(\frac{A_{open}}{A_{panel}}\right) \quad 1 \qquad \textbf{[Eq 6]}$$

Where:

A_{open} = area of the openings (in.^{2})

A_{panel} = area of the infill panel (in.^{2}) = l x h

Note: If the area of the openings (A_{open}) is greater than or equal to 60 percent of the area of the infill panel (A_{panel}), then the effect of the infill should be neglected, i.e., $(R_1)_i = 0$.

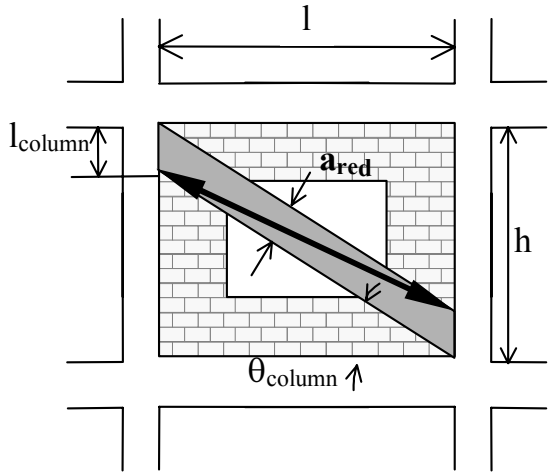

Figure 6. Perforated panel.

Note that reducing the strut width to account for an opening does not necessarily represent the stress distributions likely to occur. This method is a simplification in order to compute the global structural capacity. Local effects due to an opening should be considered by either modeling the perforated panel with finite elements or using struts to accurately represent possible stress fields as shown in Figure 7.

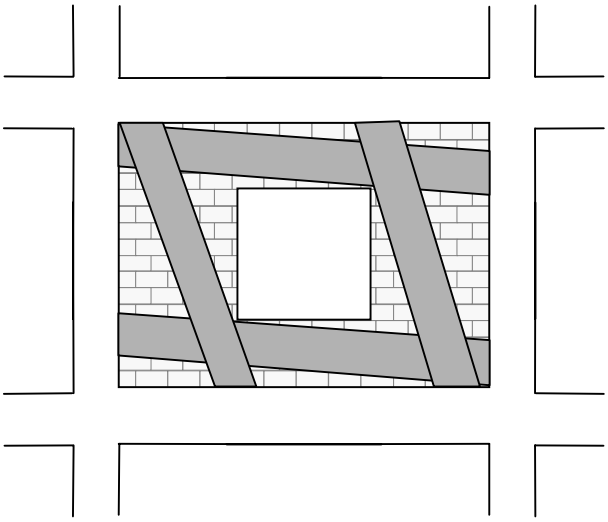

Figure 7. Possible strut placement for perforated panel.

Existing Infill Damage

Masonry infill panel behavior deteriorates as the elastic limit is exceeded. For this reason, it is important to determine whether the masonry in the panel has exceeded the elastic limit and, if so, by how much. The extent of existing infill damage can be determined by visual inspection of the infill. Existing panel

damage (or cracking) must be classified as either: no damage, moderate damage, or severe damage as presented in Figure 8. If in doubt as to the magnitude of existing panel damage, assume severe damage for a safer (conservative) estimate. A reduction factor for existing panel damage $(R_2)_i$ must be obtained from Table 2. Notice that, if the slenderness ratio (h/t) of the panel is greater than 21, $(R_2)_i$ is not defined and repair is required. For panels with no existing panel damage, the reduction factor $(R_2)_i$ must be taken as 1.0.

Table 2. In-plane damage reduction factor.

	$(R_2)_i$ for Type of Damage	
h/t	*Moderate*	*Severe*
≤ 21	0.7	0.4
> 21	Requires Repair	

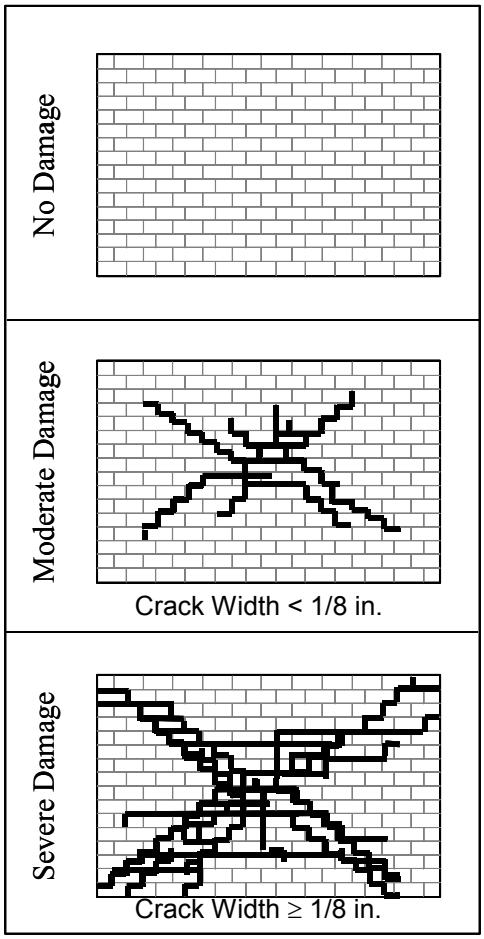

Figure 8. Visual damage classification.

Load-Deformation Behavior of the Eccentric Equivalent Strut

The eccentric equivalent strut used to model the masonry infill is pin-connected to the frame elements so that no moment transfer occurs. The stiffness of the strut will be governed by the modulus of elasticity of the masonry material *(E_m)* and the cross-sectional area (a x t_{eff}). The strength of the strut is determined by calculating the load required to reach masonry infill crushing strength (R_{cr}) (Equation 9) and the load required to reach the masonry infill shear strength (R_{shear}) (Equation 10). The component of these forces in the direction of the equivalent strut will be used to assign the strut a "compressive" strength. This strength is defined as R_{strut} (Equation 7) and governs the strength of the plastic hinge in the strut.

$$R_{strut} = \min\begin{Bmatrix} R_{cr} \\ R_{shear} / \cos\theta_{strut} \end{Bmatrix} \quad \textbf{[Eq 7]}$$

$$\tan\theta_{strut} = \frac{h - 2l_{column}}{l} \quad \textbf{[Eq 8]}$$

Where:

θ_{strut} = the angle of the eccentric strut with respect to the horizontal, given by Equation 8 and illustrated in Figure 9.

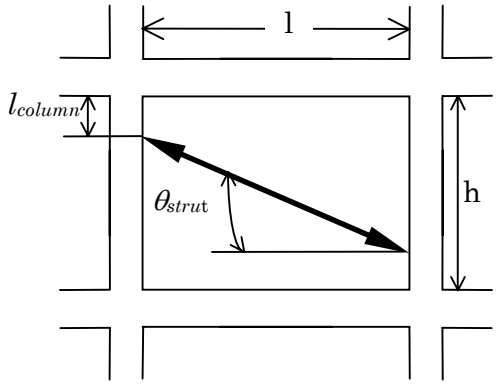

Figure 9. Geometry of θ_{strut}.

The equivalent strut is assumed to deflect to nonlinear drifts as Figure 10 shows.

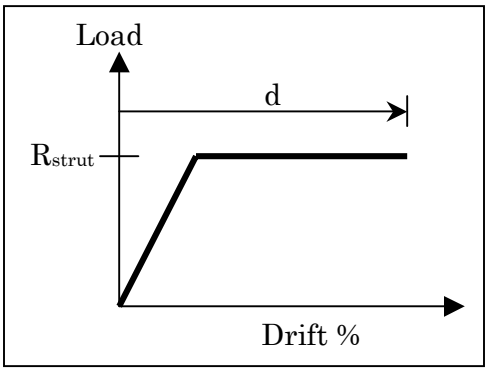

Figure 10. Load-deformation behavior.

The parameter *d*, which represents the nonlinear lateral drift associated with the infilled panel, is defined in Table 7-7 of FEMA 273.

Masonry infill crushing strength.

The masonry infill crushing strength corresponds to the compressive load that the equivalent masonry strut can carry before the masonry is crushed (R_{cr}). The applied load that corresponds to the crushing strength of the infill is evaluated using Equation 9.

$$R_{cr} = a_{red}\, t_{eff}\, f'_m \qquad \textbf{[Eq 9]}$$

Where:

f'_m = compressive strength of the masonry (psi)

t_{eff} = net thickness of the masonry panel (in)

Masonry infill shear strength.

The capacity of masonry to shear forces is provided by the combination of two different mechanisms: the bond shear strength and the friction between the masonry and the mortar. The concept of the bond shear strength is illustrated in Figure 11, where a typical stair-stepped shear crack is approximated by a single shear crack through a bed joint. This simplification is valid because the vertical component of the stair-stepped crack will be in tension, and its contribution to the shear strength should be neglected. Therefore, the horizontal lateral load required to reach the infill shear strength is calculated by Equation 10.

$$R_{shear} = A_n f'_v (R_1)_i (R_2)_i \quad \text{[Eq 10]}$$

Where:

A_n = net cross sectional mortar/grouted area of infill panel along its length (in.^{2})

f'_v = masonry shear strength (psi)

Note: Although vertical loads on infills may not be accurately estimated, 20 percent of the normal stress may be assumed to be resisted by the infill and included in the friction component of the resisting mechanism.

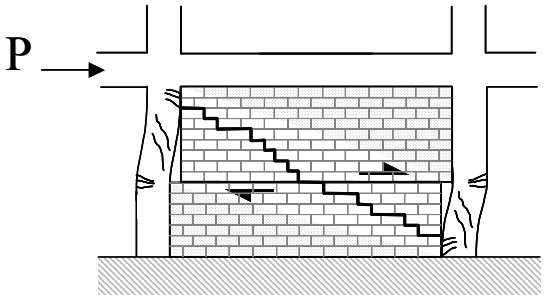

Figure 11. Shear failure of masonry.

Plastic Hinge Placement

Plastic hinges in columns should capture the interaction between axial load and moment capacity. These hinges should be located at a minimum distance l_{column} from the face of the beam. Hinges in beams need only characterize the flexural behavior of the member. These hinges should be placed at a minimum distance l_{beam} from the face of the column. This distance is calculated from Equations 11 and 12 where θ_{beam} is the angle at which the infill forces would act if the eccentricity of the equivalent strut was assumed to act on the beam as depicted in Figure 12.

$$l_{beam} = \frac{a}{\sin \theta_{beam}} \quad \text{[Eq 11]}$$

$$\tan \theta_{beam} = \frac{h}{l - \frac{a}{\sin \theta_{beam}}} \quad \text{[Eq 12]}$$

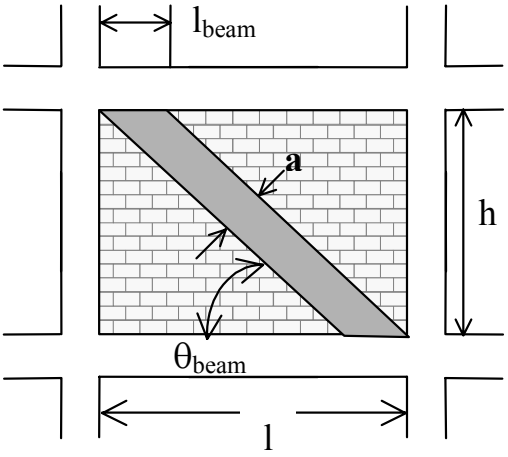

Figure 12. Distance to beam hinge.

Although the infill forces are assumed to act directly on the columns, hinging in the beams will still occur and l_{beam} is a reasonable estimate of the distance from the face of the column to the plastic hinge.

Shear hinges must also be incorporated in both columns and beams. The equivalent strut, however, only needs hinges that represent the axial load. This hinge should be placed at the midspan of the member. In general, the minimum number and type of plastic hinges needed to capture the inelastic actions of an infilled frame are depicted in Figure 13.

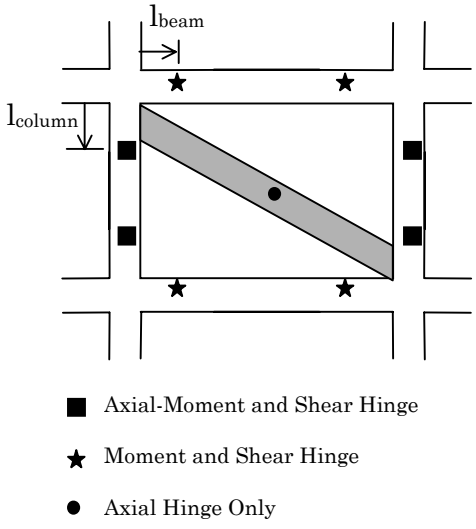

Figure 13. Plastic hinge placement.

Although lateral loading generally leads to hinge formation near the end of a member, inelastic deformation may occur at other locations, especially when large gravity loads are present. Therefore, the possibility of hinging near midspan must not be overlooked. In addition, the engineer is allowed to place hinges differently if the placement is justified and good engineering judgment is used.

Rigid End Offsets

The frame elements surrounding a panel containing an equivalent strut in the mathematical model will be too flexible. This is because of the lack of confinement produced by the strut that would have been provided had the infill been modeled with finite elements. To counteract this effect, it is recommended that REOs be placed on the frame members surrounding an infilled panel. For beams surrounding infilled panels, REOs should be used from the beam/column joint to a distance of l_{beam} from the face of the column. For columns surrounding infilled panels, REOs should be placed from the beam/column joint to a distance of l_{column} from the face of the beam. These distances also correspond to the locations of the beam and column plastic hinges. The beam or column is therefore assumed to be rigid up to the point of the plastic hinge. Figure 14 shows the placement of REOs (shown in black) for an infilled frame.

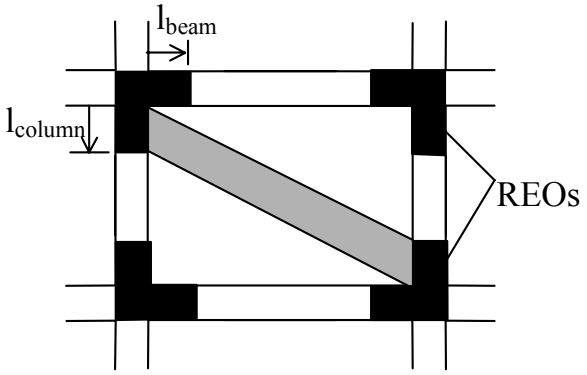

Figure 14. Rigid end offset placement.

Loading

The mathematical model should be subjected to monotonically increasing lateral loads until the maximum displacement of the design earthquake is reached or a failure mechanism forms. The target displacement should be calculated following the procedure in Section 3.3.3.3 of FEMA 273. Gravity loads should be applied as initial conditions prior to the earthquake loadings. The load combinations that should be used are given by Equations 3-2 and 3-3 in FEMA 273.

Lateral loads should be applied in a manner that approximates the inertia forces in the design earthquake. It is recommended that a minimum of two different inertia force distributions be used in order to capture the worst-case design forces. The recommended inertia force distributions are given in Section 3.3.3.2 of FEMA 273.

4 In-Plane Stiffness Evaluation of URM Infills

The following procedure should be used to resolve the stiffness of structures containing fully infilled panels, partially infilled panels, and/or perforated masonry panels. This method relies on exploiting the pushover curve generated by the structural analysis program for capacity evaluation. The pushover curve must be modified, however, to accurately represent displacements. Modifications must be made in order to increase the initial stiffness and reduce the displacement at ultimate load since the use of an equivalent strut in the pushover analysis yields mathematical models, which are more flexible than experimental models.

The general procedure for correcting the pushover curve consists of approximating the curve with a bilinear load-deflection relationship. The slopes of both segments of the bilinear curve are then increased while keeping the "yield" and ultimate loads constant. In effect, the values for initial stiffness and displacement at ultimate are modified to more reasonable values.

Bilinear Load-Deflection Behavior

The bilinear load-deflection curve is defined by three points; the origin, the "yield" load and displacement (V_y and Δ_y), and the ultimate load and displacement (V_u and Δ_u). The "yield" load, as used within this report, does not refer to any specific material yielding, but only to signify a change in stiffness represented by the bilinear load-deflection curve. The bilinear curve is also defined by two stiffnesses, K_y and K_u, which are the slopes of the initial and final portions of the curve. The bilinear curve should be drawn in a manner that minimizes the deviations from the actual pushover curve as shown in Figure 15.

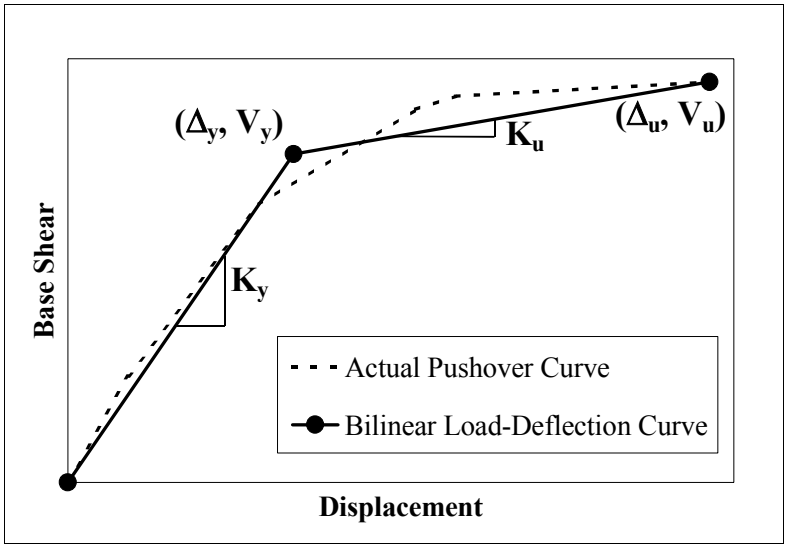

Figure 15. Bilinear load-deflection curve.

Once the bilinear curve has been drawn, it must be modified to increase the initial stiffness and decrease the displacement at ultimate load to more reasonable values. The "yield" and ultimate loads are held constant while K_y and K_u are increased to K_i and K_f, respectively. K_i represents the actual initial elastic stiffness of the infilled structure, while K_f represents the final stiffness (i.e., the stiffness from the "yield" load to the ultimate load). Figure 16 shows the modified bilinear load-deflection curve. Δ_y' represents the modified displacement at yield, while Δ_u' represents the actual displacement of the infilled structure at ultimate load.

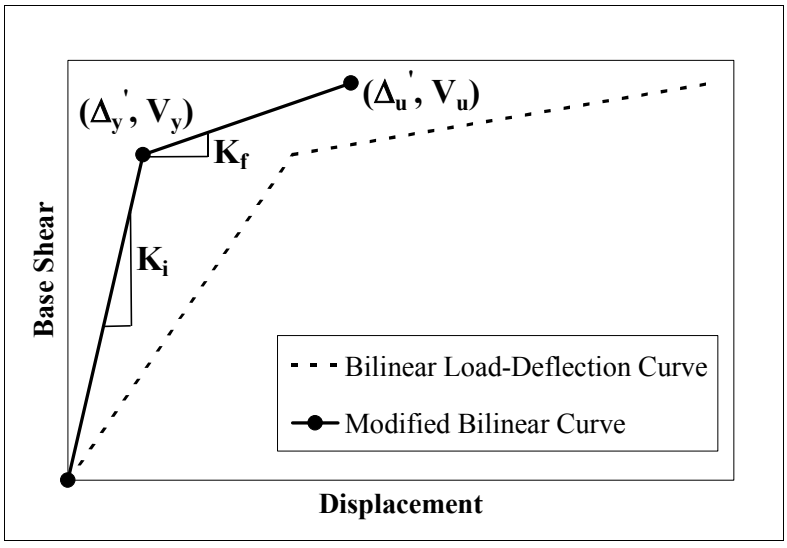

Figure 16. Modified load-deflection curve.

The modified bilinear curve better represents the initial stiffness and displacement at ultimate load for the infilled structure. The procedure for determining K_i and K_f as well as the rationale for such modifications, is discussed in the following section.

Determination of K_i and K_f

The pushover curve of a masonry-infilled structure that is modeled with eccentric equivalent struts and used to determine the *capacity* will be too flexible relative to experimental results. The initial stiffness is too small and the displacement at ultimate is too large. These results stem from the approximation when using an equivalent strut to represent a masonry-infilled panel.

The equation used to calculate the equivalent strut width for determining the capacity of the infill panel is based on a more conservative approach by Mainstone (1971), which establishes a lower bound of the expected elastic stiffness of the infill (shown by the lower curve in Figure 17). Mainstone (1971) only considered the relative infill-to-frame flexibility in the evaluation of the equivalent strut width of the panel. Upper bound estimates for elastic stiffness, according to Stafford-Smith and Carter (1969), vary not only with the relative infill-to-frame stiffness but also with the aspect ratio of the panel (l/h) as illustrated in Figure 17 (for l/h = 1.0, 1.5, 2.0, and 2.5). The largest possible values for a/d correspond to panels with aspect ratios (l/h) of 1.0. For l/h ratios smaller than 1.0, the inverse of the ratio should be used to determine the equivalent strut width.

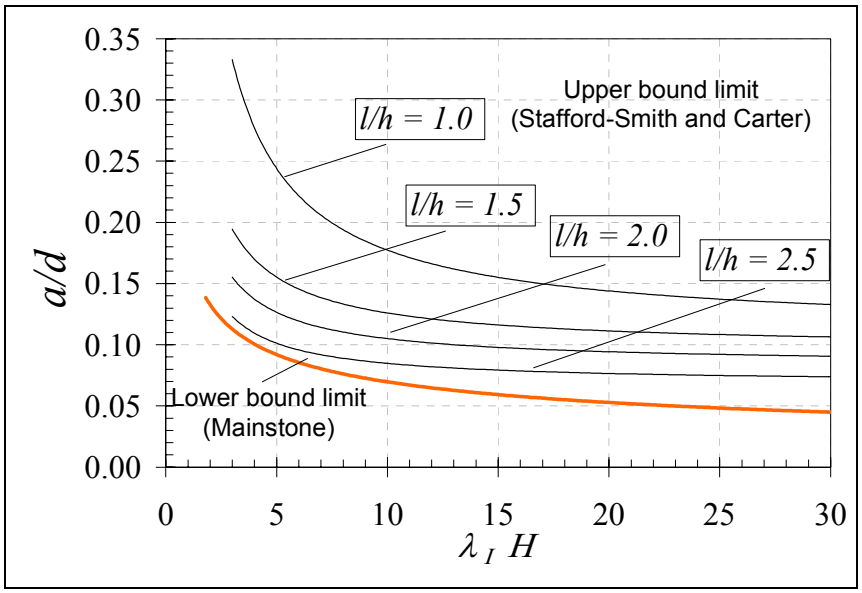

Figure 17. Upper/lower limit strut width.

Equivalent strut width estimates by Stafford-Smith and Carter (1969) may also be obtained using Equations 13 and 14, for panels with panel aspect ratios greater than or equal to 1.5. For aspect ratios of 1.0, Equation 15 must be used. Linear interpolation is allowed for panel aspect ratios between 1.0 and 1.5.

$$a \quad 0.0835CD\ 1 \quad \frac{2.574}{\lambda_1 H} \quad for\ l/h \quad 1.5 \qquad \textbf{[Eq 13]}$$

$$C = -0.3905\left(\frac{l}{h}\right) + 1.7829 \qquad \textbf{[Eq 14]}$$

$$a = 0.1106D\left(1 + \frac{6.027}{\lambda_1 H}\right) \quad for\ l/h = 1.0 \qquad \textbf{[Eq 15]}$$

From Figure 17, for aspect ratios between 1.0 and 1.5, Mainstone (1971) underestimates the strut width, a, by a significant amount. As the aspect ratio increases past 1.5, the difference in strut width estimates between Mainstone (1971) and Stafford-Smith and Carter (1969) decreases. Therefore, the initial bilinear stiffness, K_y, found from the pushover analysis and based on equations from Mainstone (1971), must be corrected to account for the inadequate stiffness provided by the strut calculated from Equation 3. The following two methods are proposed to increase the initial stiffness.

The first method increases the existing K_y by a factor of three, but is applicable only for infill panels with an aspect ratio between 0.67 and 1.5. This assumption allows the engineer to use the existing data obtained from the pushover analysis and avoid creating another mathematical model. The factor of three accounts for the difference in strut width estimates found by Mainstone (1971) compared to Stafford-Smith and Carter (1969). Note: This method is only an approximation. It is suggested to verify the calculated stiffness be verified by following the second procedure discussed next.

The second method can be used for any aspect ratio, but *must* be used for aspect ratios less than 0.67 or greater than 1.5. This method uses the equations by Stafford-Smith and Carter (1969) to calculate a strut width. Using these strut widths, a new mathematical model must be constructed and the elastic stiffness of this model should be used as the initial elastic stiffness of the infilled structure. This stiffness is referred to as K_{SSC} and represents the initial elastic stiffness determined by Stafford-Smith and Carter (1969).

The two methods are summarized in Equation 16.

$$K_i = \begin{cases} 3K_y & (0.67 \le \frac{l}{h} \le 1.5) \\ K_{SSC} & (any \quad \frac{l}{h}) \end{cases} \quad \textbf{[Eq 16]}$$

The final stiffness must also be increased in order to reduce the displacement at ultimate load to more reasonable values. Increasing the secondary stiffness from the pushover, K_u, by a factor of two along with increasing the initial stiffness to K_i and keeping the "yield" and ultimate loads constant led to displacement at ultimate load, which matched experimental values fairly well. The relationship for K_f is expressed in Equation 17.

$$K_f = 2K_u \quad \textbf{[Eq 17]}$$

Using the calculated values for K_i and K_f, the modified bilinear load-deflection relationship should reasonably predict the initial stiffness (K_i), ultimate load capacity (V_u), and displacement at ultimate load (Δ_u') of the infilled structure.

5 Out-of-Plane Evaluation of URM Infills

The out-of-plane evaluation procedure for URM infill panels presented in this report relies on the development of arching action as the primary lateral-force-resisting mechanism. The arching-action-resisting mechanism develops after cracking is observed on the masonry surface of panels that have full bonding mortar joints along the entire infill-frame boundary perimeter. Strength evaluations must consider reduction factors to take into account the presence of infill openings $(R_1)_o$, possible existing infill damage $(R_2)_o$, and the flexibility of confining frame elements $(R_3)_o$. Out-of-plane stiffness criteria are listed in the following section.

Out-of-Plane Strength and Stiffness Evaluation

URM infills may be expected to resist lateral forces as a result of wind pressures, seismic accelerations, earth pressures, etc. These lateral pressures/loads are resisted by two different mechanisms: masonry tensile strength (up to cracking in the masonry) and arching action.

Masonry behaves first as a linearly elastic material until it cracks (i.e., f_t is reached). Once the lateral cracking strength of the infill is reached, the out-of-plane load carrying capacity of the panel decreases, unless the criteria necessary to develop arching action are met.

For arching action to be considered as a resisting mechanism to out-of-plane forces in specimens, the following three criteria must be met:

- The infill panel is in full tight contact with its surrounding frame.
- The slenderness ratio (h/t) of the infill panel is not greater than 25.
- All confining beam and column elements have E_cI_{beam} and E_cI_{column} greater than $2\text{x}10^6$ k-in^2.

For panels meeting the criteria required for development of arching action, the out-of-plane lateral strength of the panel is evaluated by Equation 18. (The units for the out-of-plane strength capacity of URM infill (w) are in the same units as the masonry compressive strength (f'_m)).

$$w = \frac{2 f_m' \lambda_o}{h/t} (R_1)_o (R_2)_o (R_3)_o \qquad \text{[Eq 18]}$$

Where:

λ_o = slenderness parameter Table 3.

$(R_1)_o$, $(R_2)_o$, $(R_3)_o$ = multiplication factors that consider the presence of (see the next three sections) openings in the infill, existing panel damage, and flexibility of confining frame.

Table 3. Out-of-plane slenderness parameter.

h/t	λ_o
5	0.129
10	0.060
15	0.034
20	0.021
25	0.013

Note that Equation 18 calculates an out-of-plane capacity for the *entire* panel. Openings are accounted for by the reduction factor $(R_1)_o$. Therefore, w should be applied to the entire area of the masonry panel (including openings) to calculate the capacity in units of force.

Perforated Panels

The size and number of openings present in an infill panel can vary its stiffness as well as its strength. A reduction factor $(R_1)_0$ takes into account the effect of infill openings during the out-of-plane evaluation of infill panels and is evaluated using Equation 19.

$$(R_1)_o = \frac{5}{4}\left(1 - \frac{A_{open}}{A_{panel}}\right) \qquad \text{[Eq 19]}$$

Infills with openings of less than 20 percent of the total area of the panel may be assumed to be fully infilled for the out-of-plane evaluation ($(R_1)_o = 1$).

Existing Infill Damage

Existing infill damage must be accounted for in the in-plane evaluation. A reduction factor for existing panel damage $(R_2)_o$ must be obtained from Table 4 (linear interpolation between given values is allowed). Notice that $(R_2)_o$ depends on the level of existing panel damage and on the slenderness ratio (h/t) of the panel. For panels with no existing panel damage, the reduction factor $(R_2)_o$ must be taken as unity.

Table 4. Damage reduction factors.

	$(R_2)_o$ for Damage Level	
h/t	*Moderate*	*Severe*
5	0.997	0.994
10	0.946	0.894
15	0.888	0.789
20	0.829	0.688
25	0.776	0.602

Flexibility of Frame Elements

The elements that form the structural frame system of the building must provide enough confinement and strength for arching action to properly develop. A reduction factor $(R_3)_o$ must be considered during the out-of plane evaluation of infills, for cases where frames do not provide adequate confinement. Depending on the location of the infill panel being evaluated, the smallest confining frame element (E_cI_{column} for columns or E_cI_{beam} for beams) must be checked for compliance with a minimum value for the "Confinement" index ($E_cI_{frame} = 2.0\text{x}10^6$ k-in.^{2}).

Based on the geometrical and mechanical properties of confining frame elements, the flexibility reduction factor $(R_3)_o$ is evaluated by Equation 20 for elements with an EI_{frame} index greater than $2.0\text{x}10^6$ k-in.^{2}.

$$(R_3)_o = 0.4 + 7.1^{-8} E_c I_{frame} \qquad \textbf{[Eq 20]}$$

Where:

I_{frame} = Lesser Moment of inertia between I_{beam} and I_{column} (in.^{4})

For elements with EI_{frame} indexes greater than $9.0\text{x}10^6$ k-in.^{2}, or elements with infill continuity as explained in the following paragraph, $(R_3)_o$ may be taken as unity.

The frame elements to be checked during the evaluation of infills at different locations within a structure are presented in Figure 18. Only the frame elements that do not have infills on both sides must be evaluated. For infill #1, the smallest element between the top beam and the right and left columns must be checked. These elements do not have infill continuity on both sides. For infill #2, only the left column must be evaluated because the other three confining elements have continuity of infill on both sides. In the same way, only the top beam must be checked during the evaluation of panel #3. Because all frame elements confining panel #4 have infill continuity, the frame elements do not require evaluation and the flexibility reduction factor $(R_3)_o$ may be taken as unity (1.0).

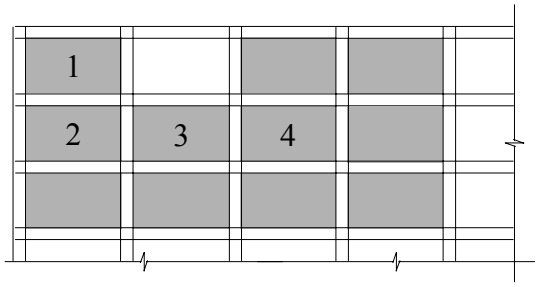

Figure 18. Infill location.

Effect of Out-of-Plane Loading on In-Plane Capacity

The effects of out-of-plane loading cannot be neglected when analyzing the in-plane capacity of an infilled structure. The in-plane capacity can be significantly reduced if large out-of-plane loads exist. Equation 21 should be used to account for this in-plane capacity reduction. This interaction formula was developed based on nonlinear finite element analysis (FEA) on infilled frames. If the out-of-plane demand is less than or equal to 20 percent of the out-of-plane capacity, however, the in-plane capacity should not be reduced and Equation 21 does not apply.

$$\frac{IP_{reduced}}{IP_{capacity}} = 1 + \frac{1}{4}\frac{OP_{demand}}{OP_{capacity}} - \frac{5}{4}\left(\frac{OP_{demand}}{OP_{capacity}}\right)^2 \qquad \textbf{[Eq 21]}$$

Where:

$IP_{reduced}$ = the in-plane capacity considering out-of-plane loading

$IP_{capacity}$ = the in-plane capacity found from the section on general procedures for evaluating the capacity of infilled frames using pushover analyses

OP_{demand} = the out-of-plane demand placed on the infilled frame.

$OP_{capacity}$ = the out-of-plane capacity found from the section on out-of-plane strength evaluation.

6 Alternative Methods of Analysis

The nonlinear static analysis procedure recommended in this document may not be available to all engineers. Therefore, an alternative linear static procedure is proposed for those individuals to use. The procedure consists of creating a linear elastic computer model of the structure. Lateral loads should be applied in a manner that approximates the inertia forces in the design earthquake. The base shear should be computed that yields demand to capacity ratios equal to or less than one for all structural members involved in resisting lateral loads. This load should then be increased by 50 percent in order to estimate the ultimate capacity of the masonry-infilled structure. The additional capacity comes from nonlinear sources such as strain-hardening effects and the progression of plastic hinging in the structure; neither of which can be captured in a linear analysis.

Other possible analysis techniques include linear and nonlinear dynamic methods. To use these methods, the asymmetry of the structure due to the orientation of the struts must be eliminated. Furthermore, the struts are assumed to act only as compression members; therefore, should not be allowed to resist tensile forces. Because of the complexities involved with solving these problems, a linear or nonlinear dynamic analysis of a masonry-infilled structure modeled with equivalent eccentric struts following the procedure in this document is not recommended.

References

Cited

Al-Chaar, G., *Non-Ductile Behavior of Reinforced Concrete Frames with Masonry Infill Panels Subjected to In-Plane Loading*, U.S. Army Corps of Engineers, Construction Engineering Research Laboratories, Technical Manuscript 99/18/ADA 360129, December 1998.

Angel, R., D.P. Abram, D. Shapiro, J. Uzarski, and M. Webster, *Behavior of Reinforced Concrete Frames with Masonry Infills*, Structural Research Series No. 589, UILU-ENG-94-2005, University of Illinois at Urbana, Illinois, March 1994.

Federal Emergency Management Agency (FEMA) 273, *NEHRP Guidelines for the Seismic Rehabilitation of Buildings*, FEMA, October 1997.

FEMA 310, *Handbook for the Seismic Evaluation of Buildings – A Prestandard,* FEMA, January 1998.

Klingner, R.E., and V. Bertero, *Infilled Frames in Earthquake-Resistant Construction*, Report No. EERC 76-32, Earthquake Engineering Research Center, University of California, Berkeley, December 1976.

Klingner, R.E., and V. Bertero, "Earthquake Resistance of Infilled Frames," *Journal of the Structural Division*, ASCE, Vol. 104, June 1978.

Mainstone, R. J., "On the Stiffness and Strength of Infilled Frames," *Proceedings of the Institution of Civil Engineers*, 1971.

Paulay, T., and M.J.N. Priestley, *Seismic Design of Reinforced Concrete and Masonry Buildings*, John Wiley & Sons, 1992.

Polyakov, S.V., "On The Interaction Between Masonry Filler Walls and Enclosing Frame When Loaded In The Plane Of The Wall," *Translations in Earthquake Engineering Research Institute*, 1960.

Stafford-Smith, B., and C. Carter, "A Method of Analysis for Infilled Frames," *Proceedings of the Institution of Civil Engineers*, Vol. 44, 1969.

Stafford-Smith, B., "Behavior of Square Infilled Frames," *Journal of the Structural Division*, ASCE, Vol. 92, February 1966.

Stafford-Smith, B., "Lateral Stiffness of Infilled Frames," *Journal of the Structural Division*, ASCE, Vol. 88, December 1962.

Uncited

Al-Chaar, G. and D. Abrams, "Parametric Studies on Seismic Behavior of Frame-Infill Systems," *Proceedings of the Ninth Canadian Masonry Symposium*, New Brunswick, Canada, June 2001.

Al-Chaar, G., G. Lamb, and D. Abrams, "Seismic Behavior of a Multistory and Multibay Frame-Infill System," *Proceedings of the Ninth Canadian Masonry Symposium*, New Brunswick, Canada, June 2001.

Angel, R. and J. Uzarski, "Estimating Transverse Strength of Masonry Infills," *Proceedings of the World Advances in Structural Concrete and Masonry Conference*, Chicago, IL, April, 1996.

Council on Tall Buildings and Urban Habitat, *Structural Design of Tall Concrete and Masonry Buildings*, Monograph, Vol. CB, 1978.

Drysdale, R.G., A.A. Hamid, and L. R. Baker, *Masonry Structures: Behavior and Design*, Englewood Cliffs, NJ, 1994.

FEMA 178, *NEHRP Handbook for the Seismic Evaluation of Existing Buildings*, FEMA, June 1992.

FEMA 274, *NEHRP Commentary on the Guidelines for the Seismic Rehabilitation of Buildings,* FEMA, October 1997.

Mallick, D.V., and R.P. Garg, "Effects of Openings on the Lateral Stiffness of Infilled Frames," *Proceedings of the Institution of Civil Engineers*, Vol. 49, June 1971.

Mehrabi, A. and M. Schuller, "Experimental Evaluation of Masonry-Infilled RC Frames," *Journal of Structural Engineering*, ASCE, Vol. 122, No. 3, March 1996.

Proceedings from the NCEER Workshop on *Seismic Response of Masonry Infill*, Technical Report NCEER-94-0004, National Center for Earthquake Engineering Research, State University of New York, Buffalo, March 1994.

Proceedings of the U.S.-Italy Workshop on *Guidelines for Seismic Evaluation and Rehabilitation of Unreinforced Masonry Buildings*, Technical Report NCEER-94-0021, National Center for Earthquake Engineering Research, State University of New York, Buffalo, July, 1994.

Riddington, J.R., "The Influence of Initial Gaps on Infilled Frame Behavior," *Proceedings of the Institution of Civil Engineers*, Part 2, Vol. 77, September 1984.

Appendix A: 3x3 Full-Scale Infilled Example

This illustrative example details the procedure for estimating the ultimate base shear capacity, deflection at ultimate capacity, and initial stiffness for an infilled reinforced concrete (R/C) frame using a structural analysis program (SAP) push-over analysis.

This example investigates the behavior of a full-scale, 3-story 3-bay R/C frame. The frame is partially infilled with door and window openings in the lower outside panel, with the remainder of the panels fully infilled. The structure will be assumed to be new, with no existing infill damage. Figure A.1 shows an elevation view of the bare frame, while Figure A.2 shows the dimensions of the openings.

Cross-section diagrams for the frame elements are illustrated in Figures A.3 and A.4, while the dimensional and physical properties of the frame, infill panel, and openings are listed in Table A.1.

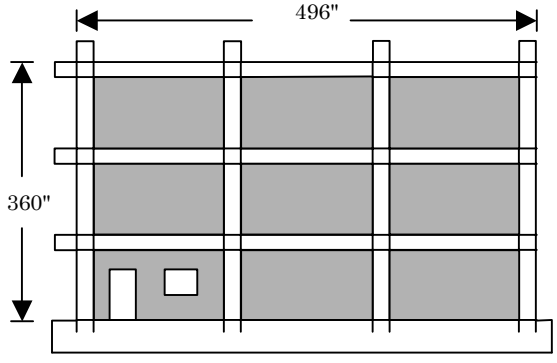

Figure A.1. Elevation view of building.

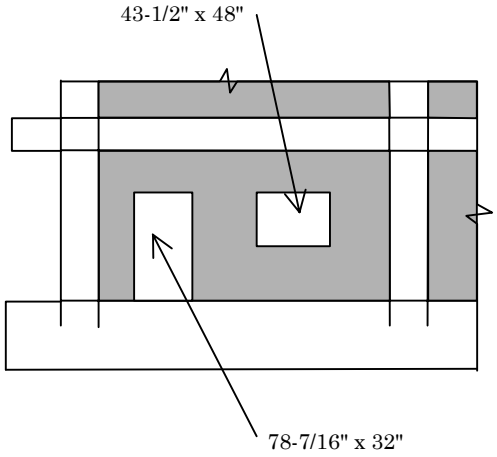

Figure A.2. Panel with openings.

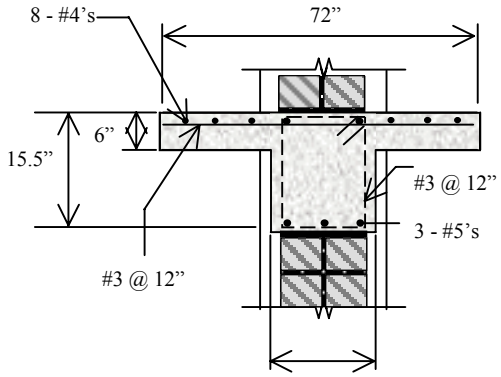

Figure A.3. Beam cross-section.

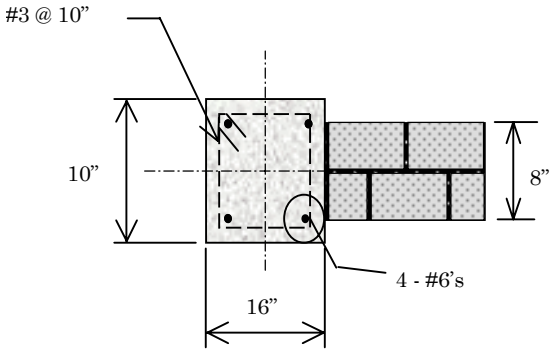

Figure A.4. Column cross-section.

Table A.1. Frame/infill properties.

Frame	Infill	Openings
E_c = 4300 ksi	E_m = 2200 ksi	h_{door} = $78^{7/16}$ in.
f'_c = 5575 psi	f'_m = 2505 psi	b_{door} = 32 in.
f_y = 60 ksi	f'_v = 265 psi	h_{window} = $43^{1/2}$ in.
h_c = 16 in.	A_n = 270.7 $in.^2$	b_{window} = 48 in.
b_c = 10 in.	H = 120 in.	A_{panel} = 15048 $in.^2$
I_c = 3413 $in.^4$	h = 104.5 in.	$A_{openings}$ = 4598 $in.^2$
h_b = 15.5 in.	l = 144 in.	
b_b = 72 in.	t = 8 in.	
b_{wb} = 10 in.	t_{eff} = 1.88 in.	
I_b = 6688 $in.^4$	D = 177.92 in.	
	θ = 0.943 rad	

Step 1: Modeling the Frame

The first step is to model the bare frame according to its proper dimensions and physical properties as listed in Table A.1. The frame should be modeled according to standard modeling procedures for R/C frames.

After modeling the bare frame, the equivalent eccentric diagonal struts are added to represent the masonry infill. Since most of the panels are fully infilled, the struts should, at first, be designed to represent full infill panels, then multiplied by a proper reduction factor to account for any openings in the infill panel.

The equivalent strut width is evaluated by first using Equation 1 to calculate the parameter $\lambda_1 H$, as shown in Equation A.1. $\lambda_1 H$ is then inserted into Equation 2 to determine the equivalent strut width, a, as illustrated in Equation. A.2. Since the infill panels are assumed to be undamaged, R_2 is taken to be 1.0.

$$\lambda_1 H = 120\left[\frac{2200 * 8 * \sin(2 * 0.943)}{4 * 4300 * 3413 * 104.5}\right]^{1/4}$$
$$\Rightarrow \quad \lambda_1 H = 4.877 \qquad \textbf{[Eq A.1]}$$

$$a = 0.175 * 177.92(4.877)^{-0.4}$$
$$\Rightarrow \quad a = 16.52\ in \qquad \textbf{[Eq A.2]}$$

Next, the eccentric placement for the strut must be determined by calculating the distance (l_{column}). The distance (l_{column}) is found by simultaneously solving Equations 4 and 5 for l_{column} and θ_{column}, as shown in Equations A.3 and A.4.

$$l_{column} \quad \frac{16.52}{\cos(\theta_{column})}$$

$$\tan(\theta_{column}) \quad \frac{104.5 \quad \frac{16.52}{\cos(\theta_{column})}}{144} \qquad \textbf{[Eq A.3 \& A.4]}$$

$$l_{colum} \quad 19.20\ in$$

$$\theta_{column} \quad 0.535\ rad$$

The equivalent diagonal struts should therefore be placed at a distance of 19.20 in. along the column from the beam-column joints with moment releases at each end.

The strut should be defined as a concrete material with the same material properties as the masonry panel.

Next, a strut reduction factor, $(R_1)_i$, is applied to represent the bottom-left panel with door and window openings. This factor is computed using Equation 6 then the reduced strut width is calculated from Equation 3, as shown in Equations A.5 and A.6.

$$(R_1)_i = 0.6\left(\frac{4598}{15048}\right)^2 - 1.6\left(\frac{4598}{15048}\right) + 1.0 \qquad \textbf{[Eq A.5]}$$

$$\Rightarrow \quad (R_1)_i = 0.567$$

$$a_{red} \quad 16.52 * (0.567) * (1.0)$$

$$a_{red} \quad 9.37\ in \qquad \textbf{[Eq A.6]}$$

Next, plastic hinges are defined to represent possible failure points for the frame. Hinges controlled by the combination of axial, moment, and shear forces are placed at a distance (l_{column}) from the joints along the columns. Conversely, hinges along the beam account for only moment and shear forces, and are placed at a distance (l_{beam}) from the joints. This distance (l_{beam}) is calculated by simultaneously solving Equations 11 and 12, as shown in Equations A.7 and A.8.

$$l_{beam} = \frac{16.52}{\sin(\theta_{beam})}$$

$$\tan(\theta_{beam}) = \frac{104.5}{144 - \frac{16.52}{\sin(\theta_{beam})}} \qquad \textbf{[Eq A.7 \& A.8]}$$

$$\Rightarrow \quad l_{beam} = 25.03\ in$$

$$\Rightarrow \quad \theta_{beam} = 0.721\ rad$$

Single hinges controlled only by axial forces are placed at the midpoints of the struts. Figure A.5 shows the hinge types and placement around a sample panel.

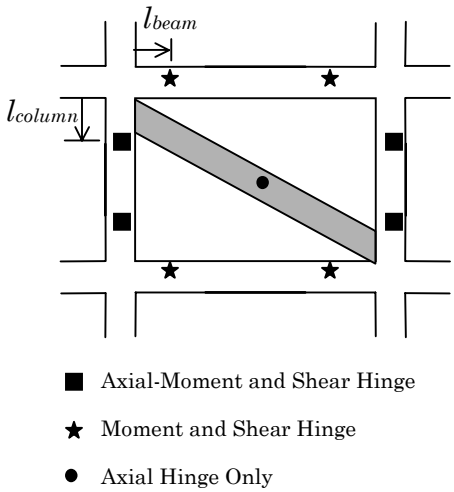

Figure A.5. Plastic hinge placement.

Upon placement of the hinges, the capacity of the strut hinges (R_{strut}) should be computed. The compressive strength (R_{strut}) should be calculated using Equations 7-10, as illustrated in Equations A.9-A.12.

$$R_{cr} = 16.52 * 1.88 * 2.505$$
$$\Rightarrow \quad R_{cr} = 77.8\ kips \qquad \textbf{[Eq A.9]}$$

$$R_{shear} = 270.7 * 0.265 * 1 * 1$$
$$\Rightarrow \quad R_{shear} = 71.7\ kips \qquad \textbf{[Eq A.10]}$$

$$\tan(\theta_{strut}) = \frac{104.5 - 2 * 19.20}{144}$$
$$\Rightarrow \quad \theta_{strut} = 24.66° \qquad \textbf{[Eq A.11]}$$

$$R_{strut} = \min\left\{\begin{matrix} 77.8\ kips \\ 71.7 \big/ \cos(24.66°) = 78.9\ kips \end{matrix}\right\} \qquad \textbf{[Eq A.12]}$$
$$\Rightarrow \quad R_{strut} = 77.8\ kips$$

Next, rigid end offsets (REOs) are placed to increase the rigidity of the joints, as well as ensure that the maximum stresses computed are located at the defined plastic hinges. The REOs should have a rigid zone factor of one and span from the beam column joints outward to a distance (l_{beam}) along the beams and a distance (l_{column}) along the column.

Finally, the load and pushover cases are defined. The pushover is defined using the local redistribution member unloading method, with gravity loads as an initial condition. The inertia force distribution from the design earthquake are represented by the lateral loads shown in Figures A.6 and A.7 for the two pushover cases. Although more than one inertia force distribution is recommended, only one is shown in this example for simplicity. Note: The two loading cases shown here were required to represent the asymmetric configuration of the openings.

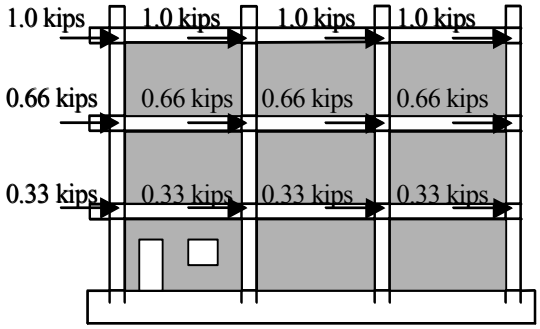

Figure A.6. Pushover Case I.

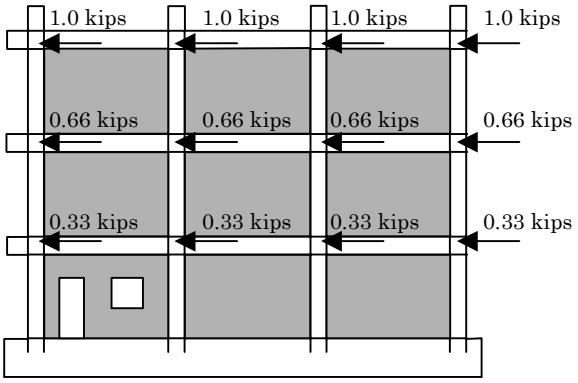

Figure A.7. Pushover Case II.

Alternatively, the Stafford-Smith and Carter (1969) set of equations can be used to calculate an alternative strut width (a_{ssc}). This strut width is calculated by first substituting the value obtained from Equation A.1 into Equations 13-15 to determine the strut width (a_{ssc}) for aspect ratios (l/h) of 1.5 and 1.0, as shown in Equations A.13-A.15.

$$C = -0.3905(1.5) + 1.7829$$
$$\Rightarrow \quad C = 1.197 \qquad \textbf{[Eq A.13]}$$

$$a_{SSC} = 0.0835 * 1.197 * 177.92\left(1 + \frac{2.574}{4.877}\right)$$
$$\Rightarrow \quad a_{SSC} = 27.17\ in \quad for\left(l/h\right) \geq 1.5 \qquad \textbf{[Eq A.14]}$$

$$a_{SSC} = 0.1106 * 177.92\left(1 + \frac{6.027}{4.877}\right)$$
$$\Rightarrow \quad a_{SSC} = 44.00\ in \quad for\left(l/h\right) = 1.0 \qquad \textbf{[Eq A.15]}$$

After obtaining strut widths for these aspect ratios, it is necessary to interpolate to determine the appropriate strut width (a_{SSC}) for this structure, as shown by Equation A.16.

$$a_{SSC} = 44.00 - \frac{\frac{144}{104.5} - 1.0}{1.5 - 1.0}(44.00 - 27.17)$$
$$\Rightarrow \quad a_{SSC} = 31.28\ in \quad for\left(l/h\right) = 1.378 \qquad \textbf{[Eq A.16]}$$

Next, the reduced strut width (a_{SSCred}) is determined by first calculating $(R_1)_i$ from Equation 6 and applying it to Equation 3, as shown in Equations A.17 and A.18.

$$(R_1)_i = 0.6\left(\frac{4598}{15048}\right)^2 - 1.6\left(\frac{4598}{15048}\right) + 1$$
$$\Rightarrow \quad (R_1)_i = 0.567 \qquad \textbf{[Eq A.17]}$$

$$a_{SSCred} = 31.28 * (0.567) * (1.0)$$
$$\Rightarrow \quad a_{SSCred} = 17.74\ in \qquad \textbf{[Eq A.18]}$$

At this point, values for l_{beam}, l_{column}, and R_{strut} must be determined similarly to those same calculations for the Mainstone (1971) strut width, with their values listed in Table A.2.

Table A.2. Stafford-Smith and Carter modeling values.

I_{beam}	47.43 in
I_{column}	36.38 in
R_{cr}	77.8 kips
R_{shear}	71.7 kips
θ_{strut}	12.44°
R_{shear}/θ_{strut}	78.9 kips
R_{strut}	77.8 kips

These values calculated from Stafford-Smith and Carter (1969) will be used only to calculate an alternate initial stiffness for the loading case that yields the lower ultimate capacity.

Step 2: Analyze Results

After running the static pushover analyses for both Case I and Case II, the lesser value for ultimate capacity is assumed as a worst-case scenario. For this example, Case I controls the ultimate capacity with a value of 152.0 kips. The static pushover curves are illustrated in Figures A.8 and A.9 for pushover Cases I and II, respectively.

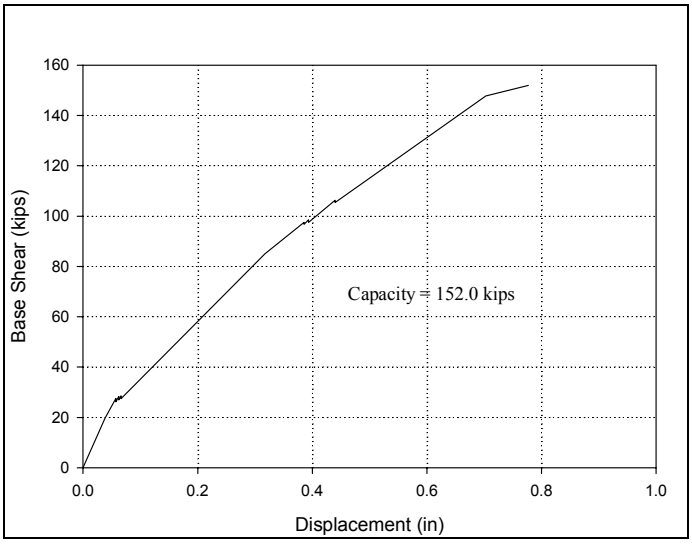

Figure A.8. Case I pushover curve.

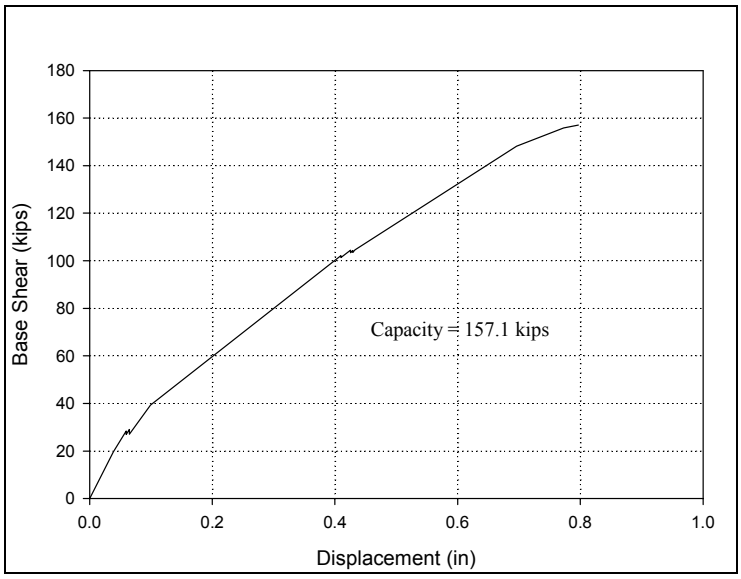

Figure A.9. Case II pushover curve.

The next step is to simplify the pushover curve as a bilinear curve with initial and post-yield stiffness values, as well as well-defined yield and ultimate values. Figure A.10 shows a plot showing the original pushover curve and its corresponding bilinear estimation.

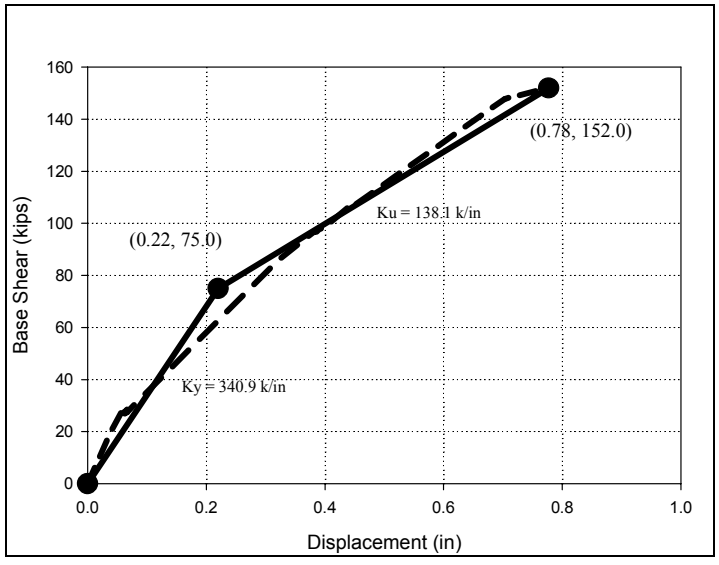

Figure A.10. Bilinear estimation.

Also shown in Figure A.10 are the initial and post-yield bilinear stiffness values for the estimated curve. For this example it is all right to use the initial stiffness value predicted using the Mainstone (1971) equations since the aspect ratio (l/h) for the panels in this frame is 1.38 (between 0.67 and 1.5). Therefore, these values are inserted into Equations 16 and 17 to determine values of K_i and K_f, as shown in Equations A.19 and A.20.

The initial linear elastic stiffness computed using the Stafford-Smith and Carter (1969) equivalent strut width equations is also included in Equation 16 as an alternate value for K_i.

$$K_i \quad 3*340.9 \quad 1023\ k/in.$$
$$1244\ k/in \qquad \textbf{[Eq A.19]}$$
$$K_i \quad 1020\ kips/in.$$

$$K_f \quad 2*138.1$$
$$K_f \quad 276\ kips/in. \qquad \textbf{[Eq A.20]}$$

Assuming the value for K_i to be 1,020 k/in., the new stiffness values are then applied, along with the estimated yield and ultimate base shear values from Figure A.10, to generate the modified bilinear plot depicted in Figure A.11. This plot should predict the in plane ultimate capacity and displacement at ultimate capacity with reasonable accuracy. The values, as defined in Figure 16, are listed in Table A.3.

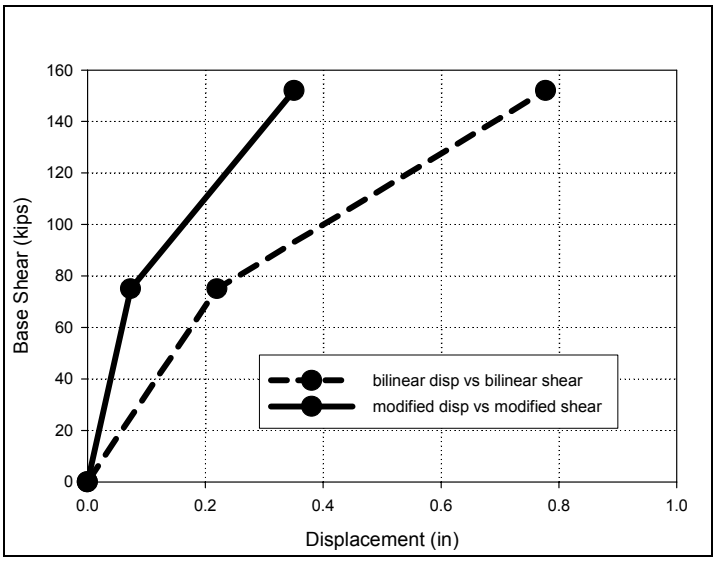

Figure A.11. Modified bilinear curve.

Table A.3. Modified stiffness, base shear, and deflections.

K_i	1020 k/in.
K_f	278 k/in.
Δ_y'	0.0735 in.
Δ_u'	0.35 in.
V_y	75.0 kips
$IP_{capacity}$	152.0 kips

Step 3: Out-of-Plane Capacity

The next step in predicting the response of the structure in question is to estimate its out-of-plane strength. First, a check is performed to determine whether arching action can be considered as a resisting mechanism to the out-of-plane forces. If the three criteria outlined in the section on out-of-plane strength evaluation are met, then arching action can be considered. For the structure in question:

1. The infill panel *is* in full tight contact with its surrounding frame.
2. The slenderness ratio (h/t) of the infill panel is 13.06, which is *not* greater than 25.
3. The confining beam and column elements have E_cI_{beam} and E_cI_{column} of 28.8x10^6 and 14.7x10^6 k-in^2 respectively, which *are* greater than 2x10^6 k-in^2.

Therefore, the out-of-plane lateral strength of the panel with openings is computed using Equation 18 as illustrated in Equation A.21. In this case $(R_2)_0$ and $(R_3)_0$ are taken as 1.0 since the structure is assumed to be undamaged and the EI_{frame} indexes are both greater than 9.0x10^6 k-in.^{2}. The value for the parameter λ_0 is taken as 0.044 as interpolated from Table 3, while $(R_1)_0$ is calculated from Equation 19, as shown in Equation A.22.

$$w = \frac{2 * 2505 * 0.044}{104.5/8}(0.868)(1.0)(1.0) \quad \Rightarrow \quad w = 14.6\ psi \qquad \textbf{[Eq A.21]}$$

$$(R_1)_0 = \frac{5}{4}\left(1 - \frac{4598}{15048}\right) \quad \Rightarrow \quad (R_1)_0 = 0.868 \qquad \textbf{[Eq A.22]}$$

So the limiting out-of-plane capacity of this structure is 14.6 psi, or when translated into units of force, 219.7 kips.

Step 4: Effect of Out-of-Plane Loading on In-Plane Capacity

Assuming a value of roughly half the out-of-plane capacity, the reduced in-plane capacity is computed using Equation 21, as shown in Equation A.23. Table A.4 summarizes the out-of-plane demand and the in-plane and out-of-plane capacities.

$$\frac{IP_{reduced}}{152.0} = 1 + \frac{1}{4}\frac{110.0}{219.7} - \frac{5}{4}\left(\frac{110.0}{219.7}\right)^2 \quad \textbf{[Eq A.23]}$$

$$\Rightarrow \quad IP_{reduced} = 123.4 \; kips$$

Table A.4. Capacity summary.

$IP_{reduced}$	123.4 kips
$IP_{capacity}$	152.0 kips
OP_{demand}	110.0 kips
$OP_{capacity}$	219.7 kips

Appendix B: Commentary on Selected Sections — Evaluating Strength and Stiffness of URM Infill Structures

Predicting Ultimate Capacity of Infilled Frames Using Pushover Analysis

Eccentric equivalent struts were chosen for this study because, when an infilled frame is loaded laterally, the columns take the majority of the forces exerted on the frame by the infill. Furthermore, the loss of a column is much more detrimental to a structure than the loss of a beam. Therefore, for ultimate capacity purposes, failure was assumed to occur when the columns failed from the infill forces. These forces act as a result of separation of the frame from the infill due to lateral loading.

The equivalent struts were estimated using equations derived by Mainstone (1971) rather than Stafford-Smith and Carter (1969). When assigning strength parameters according to Stafford-Smith and Carter's method (SSC) for estimating equivalent struts, the large strut width resulted in the development of large, unrealistic capacities, especially in the 1-story, single-bay half-scale models. Figure B.1 shows the base-shear vs. deflection curves for these models. The two plots reach an initial ultimate capacity early before hinging occurs first in the beam, then in the columns. At this point, the strut controls the strength and nearly three times the experimental ultimate load can be taken before failure occurs. The smaller Mainstone (1971) strut was therefore adopted to represent capacity.

The location of the plastic hinges is very important to the ultimate capacity of the pushover. Other locations could be used, however, depending on the structure in question. Hinges in the beams should be controlled by the member's flexural behavior, while hinges in the columns need to account for the combination between flexure and axial loads. On the other hand, due to the pinned-pinned connection assumed for the struts, only axial forces should control these plastic hinges.

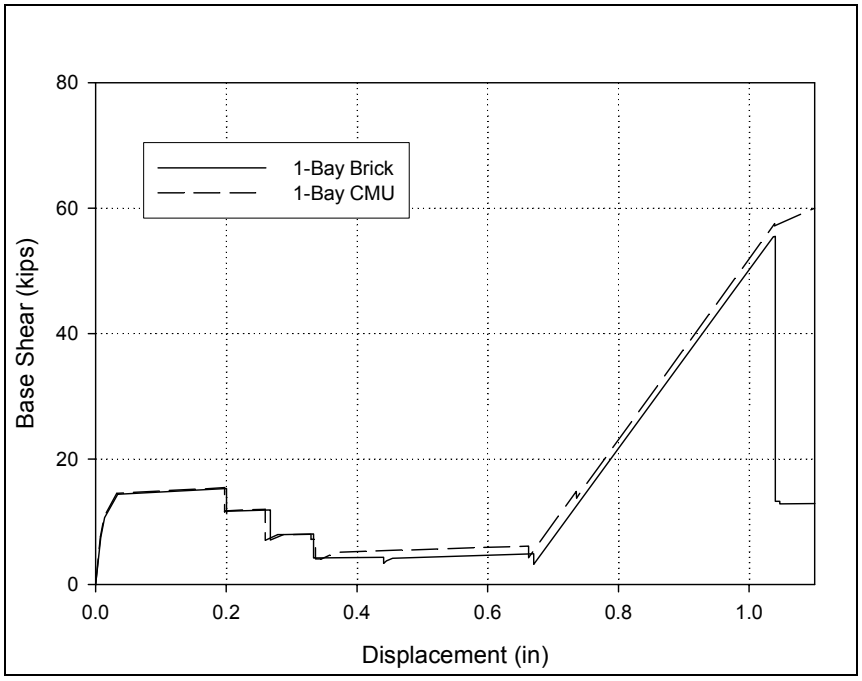

Figure B.1. Load vs. deflection (SSC).

When defining the static pushover cases, any member unloading (force redistribution upon hinge failure) method is acceptable. Table B.1 shows pushover ultimate capacities calculated by both the local redistribution and entire structure unloading methods for each of the full-scale models with complete openings and concentrated in-plane (CIP) loading. Clearly, the difference between the two member unloading methods is negligible since the largest difference is only 0.53 percent, with an average of only 0.19 percent for the 10 models.

Table B.1. Member unloading method comparison.

Opening Location	Pushover Capacity (K)		% Difference
	Local Redistribution	Unload Structure	
---	226.8	227.7	0.38
3A	227.5	227.9	0.16
3B	224.9	225.3	0.16
3C	225.8	226.2	0.17
2A	210.9	210.8	0.03
2B	212.8	212.8	0.00
2C	213.0	212.3	0.34
1A	176.4	176.4	0.00
1B	179.4	180.3	0.53
1C	178.8	179	0.13

As illustrated in Table B.2, the proposed method yields reasonable approximations for ultimate capacity when compared with experimental and nonlinear FE analyses. For the full-scale models with complete openings and CIP loading, 70 percent of the pushover models projected ultimate capacities that were within 6 percent of those calculated by FEA, with an average difference of only 6.8 percent. Furthermore, the pushover analysis predicted the ultimate capacity of the 3x3 fully infilled half-scale model to within 4.4 percent of the value obtained experimentally. Conversely, the pushover analysis was not quite as accurate with its projections for the 1-story models, ranging between 16.0 and 49.8 percent of the experimental values. (Note: The 1-story models were loaded monotonically as opposed to the cyclically loaded 3x3 experimental models.)

Table B.2. Ultimate capacity summary.

Full-Scale Models with Complete Openings and CIP Loading				
Opening Location	**Lateral Load**	**Nonlinear FEA (K)**	**Pushover Results (K)**	**% Difference**
---	CIP	222.1	227.7	2.5
3A	CIP	219.4	227.9	3.9
3B	CIP	213.2	225.3	5.7
3C	CIP	207.8	226.2	8.9
2A	CIP	206.4	210.8	2.1
2B	CIP	205.45	212.8	3.6
2C	CIP	200.45	212.3	5.9
1A	CIP	181.25	176.4	2.7
1B	CIP	160.5	180.3	12.3
1C	CIP	148.5	179	20.5
Half-Scale Models				
Model Description		**Exp. Results (K)**	**Pushover Results (K)**	**% Difference**
3x3 fully infilled		32.22	33.63	4.4
1 Bay Brick		19.83	15.94	-19.6
1 Bay CMU		18.87	15.85	-16.0
2 Bay CMU		70.13	35.2	-49.8
3 Bay Brick		82.63	56.8	-31.3
1 Bay Bare		7.7	6.35	-17.5

Perforated Panels

When the Nonlinear Finite Element Models were run for the distributed in-plane loading case (DIP), they were done so using a shear coefficient that had not been calibrated with experimental results. Once the actual experiments were performed, the shear coefficient was modified in order for the FE models to agree with the experimental results. The new shear coefficient was used in 3x3 full-scale FE models, each containing one completely open panel in different locations. The only direct correlation between the shear coefficients was on a 3x3 R/C frame fully infilled with a concrete masonry unit (CMU) full-scale model subjected to CIP loading. For this FE model, the original shear coefficient overestimated the capacity by approximately 12 percent (222.1 kips vs. 249 kips). This FE model was the only model analyzed with *both* shear coefficients. Unfortunately, a set of models was never run with the corrected shear coefficient for the DIP loading case. It was therefore necessary to "correct" the available ultimate load capacity values with DIP loading.

Reducing the capacity of each FE model by 11 percent unfortunately did not seem rational for each of the different opening configurations. Table B.3 gives a breakdown of the percent of fully infilled for each of the opening configurations for both the CIP and DIP loading cases. It is clear that the relationship between the two is nonlinear as are the percent distributions of each. Also a simple 11 percent reduction would result in elevated values for fully infilled frames with door/window openings in the third floor. Changing the loading from CIP to DIP for the fully infilled FE model, for instance, would result in a 15 percent increase in ultimate capacity (222 kips vs. 255 kips) if a simple 11 percent reduction were used. Furthermore, for openings in panel 1B, a 30 percent increase in capacity would have occurred simply due to a change in loading and opening size. In addition, using an 11 percent reduction would translate to a bare frame capacity of 26 kips, a huge underestimation. Therefore, a nonlinear relationship between the original and corrected shear coefficient needed to be found.

To estimate ultimate load values for the DIP loading case with the corrected shear coefficient, the assumption was made that a pushover analysis accurately predicts the ultimate load for both bare and fully infilled R/C frames. This assumption was reasonable since it agreed with the experimental results for a half-scale 3x3 fully infilled R/C frame within 4.4 percent, it agreed with the FEA for a similar full-scale frame within 2.5 percent, and it agreed with the experimental results of a half-scale 1-story bare frame within 17.5 percent. These values are tabulated in Table B.4.

Table B.3. Summary of % fully infilled.

Panel with Opening	Capacity (K) with CIP Loading w/ complete openings	CIP Loading % of Fully Infilled
---	222.1	100.0
3A	219.4	98.8
3B	213.2	96.0
2A	206.4	92.9
2B	205.5	92.5
1A	181.3	81.6
1B	160.5	72.3

Panel with Opening	Original Capacity (K) with DIP Loading w/ door/window openings	DIP Loading % of Fully Infilled	11% Reduced Capacity (K) with DIP Loading
---	286.8	100.0	255
3A	268.8	86.8	239
3B	262.8	78.7	234
2A	244.8	93.7	218
2B	276	91.6	246
1A	228	85.4	203
1B	232.8	96.2	207

Table B.4. Pushover predictions.

Scale	Model Description	Pushover Capacity (K)	FEA/Experimental Capacity (K)	% Difference
half	3x3 fully-infilled	33.63	32.22	**4.4**
full	3x3 fully-infilled	227.7	222.1	**2.5**
half	1-story bare	6.35	7.7	**17.5**

Next, a plot was constructed with the ultimate load as predicted by FEA on the abscissa and a factor, equal to the pushover ultimate load divided by the FEA ultimate load, on the ordinate. Since this plot would be nonlinear, a bare minimum of three points would be needed to describe this relationship with reasonable accuracy. The three points that were used are shown in Table B.5: a bare frame with CIP loading, a fully infilled frame with CIP loading, and a fully infilled frame with DIP loading. Table B.5 illustrates that the original shear coefficient overestimated the capacity for fully infilled frames while underestimating the capacity of bare frames. These cases were chosen for their accurate correlation and because both FEA and pushover data were available. The goal was to find an equation to correct for the change in shear coefficient of the finite element analyses for the DIP loading case.

Table B.5. Plot data.

Model Description	Loading Type	FEA Ultimate Capacity	Pushover Capacity / FEA Capacity
3x3 bare frame	CIP	29.4	**2.32**
3x3 fully-infilled frame	CIP	249	**0.892**
3x3 fully-infilled frame	DIP	286.8	**0.783**

With only three points to fit curves to, logarithmic, exponential, and power trend lines were very different. Guidelines were therefore chosen to decide which curve gave the best representation:

1. The capacity of all FE models with openings should be less than the fully infilled capacity.
2. The capacity of the FE models with door/window openings in floor one should be less than 90 percent of the fully infilled capacity.
3. The capacity of the models with door/window openings in the first and second floors should be greater than that of models containing complete openings in similar locations.

Using these guidelines, the power curve stood out as the best choice since it was the only one that adhered to all three guidelines. The exponential curve failed both the first and second guidelines while the logarithmic curve did not meet guideline #2. Figure B.2 shows the curves and their equations with exponential in black, logarithmic in red, and power in blue.

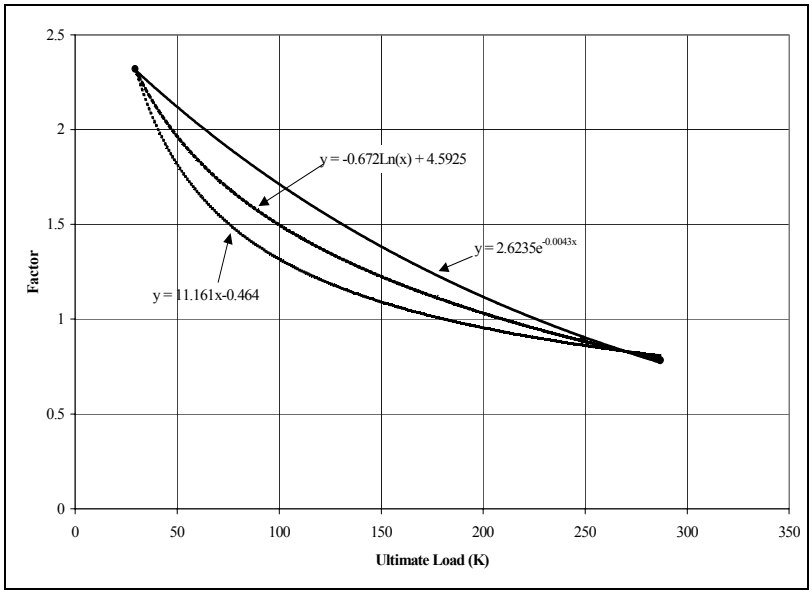

Figure B.2. Capacity vs correction factor.

The "Adjusted Load Using Power Curve" values highlighted in green in Table B.6 are assumed to be the correct FEA values for DIP loading with the corrected shear coefficient. Table B.6 shows the adjusted capacities for each of the three curves with those values not in compliance with guideline #1 highlighted in yellow, while Table B.7 tabulates the percent of fully infilled with those values that do not meet the criteria of guideline #2 also highlighted in yellow.

To determine what strut thickness to use when openings are present in an infill panel, it is necessary to determine a strut width reduction factor to multiply to the "original strut width" for a fully infilled panel. Pushover analyses were run for full-scale 3-bay by 3-story R/C infilled frames containing perforated panels. The strut widths were modified until ultimate load capacities given matched those given by FEA. The FEA data used for this relationship were corrected to account for a change in shear coefficient once experimental results were calibrated.

Table B.6. Adjusted capacities.

Opening Description	Panel with Opening	Adjusted Load Using Exp Curve (k)	Adjusted Load Using Log Curve (k)	Adjusted Load Using Power Curve (k)
fully infilled	---	219.2	226.5	**231.7**
door/window	3A	**222.0**	224.0	**223.8**
door/window	3B	**222.7**	223.0	**221.1**
door/window	2A	**224.1**	219.4	**212.9**
door/window	2B	**221.0**	225.1	**227.0**
door/window	1A	**224.4**	215.2	**204.9**
door/window	1B	**224.4**	216.5	**207.2**
large	all	145.6	129.3	**114.8**
small	all	214.0	193.1	**174.0**
no infill	all	68.0	68.2	**68.3**

Table B.7. Percent of fully infilled.

Opening Description	Panel with Opening	% of Fully Infilled Using Exp Curve	% of Fully Infilled Using Log Curve	% of Fully Infilled Using Power Curve
fully infilled	---	100.0	100.0	100.0
door/window	3A	101.3	98.9	96.6
door/window	3B	101.6	98.5	95.4
door/window	2A	102.3	96.9	91.9
door/window	2B	100.8	99.4	98.0
door/window	1A	102.4	95.0	88.4
door/window	1B	102.4	95.6	89.4
large	all	66.4	57.1	49.6
small	all	97.6	85.2	75.1
no infill	all	31.0	30.1	29.5

Six points were plotted to find a correlation between percent of open infill and percent of original strut width with the former on the abscissa and the latter on the ordinate. Only uniform and first-floor door/window opening frames were used since they were the only frames that showed significant changes in ultimate capacity. Pushover models containing upper floor door/window openings showed small changes in ultimate capacity and sometimes even increased capacity over a fully infilled frame, as shown in Table B.8. Therefore, these frames were not used as a basis. The data points that were used are tabulated in Table B.9 followed by the their plot shown in Figure B.3. The numerical interpretation of this plot becomes Equation 6:

$$(R_1)_i \quad 0.6 \frac{A_{open}}{A_{panel}}^2 \quad 1.6 \frac{A_{open}}{A_{panel}} \quad 1$$

Table B.8. Summary of discarded data.

Opening Location	Opening Description	Corrected* Nonlinear FEA Capacity (K)	Pushover Capacity (K)
---	---	231.7	224.5
3A	door/ window	223.8	224.6
3B	door/ window	221.1	225.5
2A	door/ window	212.9	212.4
2B	door/ window	227.0	211.4

Table B.9. Summary of data points.

	Area of Openings / Area of Panel	Reduced Strut Width / Original Strut Width
Bare Frame	1	0
Large Openings	0.52	0.32
1A Door/ Window	0.31	0.52
1B Door/ Window	0.31	0.63
Small Openings	0.22	0.68
Fully Infilled	0	1

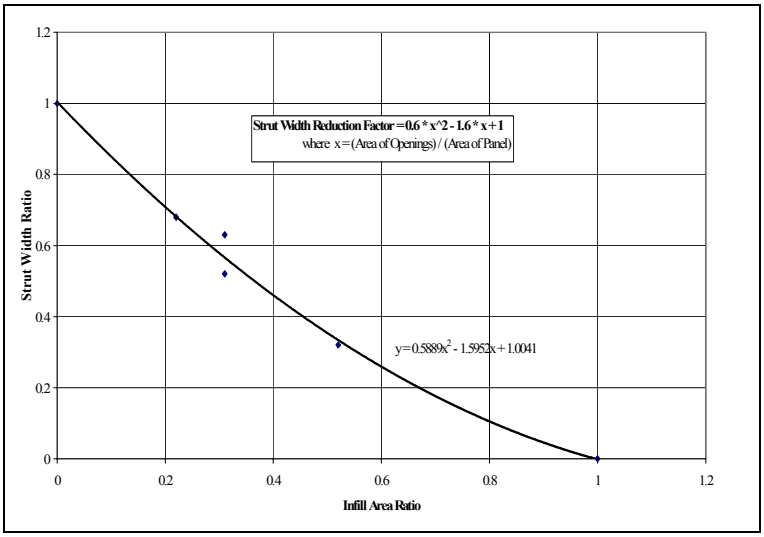

Figure B.3. Strut width vs. infill area.

A second-degree polynomial trend line fit the data series very well, giving an equation for Strut Width Reduction Factor in terms of Infill Area Ratio shown in Figure B.3. This equation was applied to determine modified strut widths for the 3x3 R/C frame with CMU infill for various opening configurations. Pushover analyses were then run for these models with the modified strut widths and compared with those values of ultimate load capacity given by FEA with a maximum error of 12.1 percent but with most being within 5 percent. These pushover capacities and their corresponding percent differences are tabulated in Table B.10.

Table B.10. Capacities from modified struts.

Opening Location	Opening Description	Corrected* Nonlinear FEA Capacity (K)	Pushover Capacity (K)	% Difference
---	---	231.7	224.5	**3.1**
3A	door/window	223.8	224.4	**0.3**
3B	door/window	221.1	225.0	**1.8**
2A	door/window	212.9	207.5	**2.5**
2B	door/window	227.0	199.5	**12.1**
1A	door/window	204.9	192.1	**6.2**
1B	door/window	207.2	188.5	**9.0**
all	large window	114.8	116.4	**1.4**
all	small window	174.0	172.7	**0.7**

Note: If the area of the openings exceeds 60 percent of the area of the infill panel, the effect of the infill should be neglected and the strut width reduction factor should be set to zero.

In-Plane Stiffness Evaluation of URM Infills

Equivalent strut width estimates calculated from both Mainstone (1971) and Stafford-Smith and Carter (1969) were implemented in the pushover analyses to determine initial stiffness and displacement at ultimate load. The Mainstone (1971) estimate is a generalized, conservative, lower bound limit represented by Equations 1 and 2:

$$\lambda_1 H = H\left[\frac{E_m t \sin 2\theta}{4E_c I_{column} h}\right]^{1/4}$$

$$a = 0.175d\left(\lambda_1 H\right)^{-0.4}$$

Unlike the Mainstone (1971) equations, the Stafford-Smith and Carter (1969) equations account for varying aspect ratios. They do so by representing their findings with four curves for aspect ratios (l/h) equal to 1.0, 1.5, 2.0, and 2.5 (should use the inverse of l/h for aspect ratios less than 1.0). These curves translate into Equations B.1-B.4, respectively, with linear interpolation for aspect ratios that fall between these values. Upon inspection of these curves, it became clear that, with the exception of the curve for aspect ratio equal to 1.0, the other curves showed a common trend. Therefore, for simplification, these three equations were transformed into a generalized equation (Equation 13), leaving Equations 13-15 as a condensed, numerical form of the Stafford-Smith and Carter (1969) curves. Figure B.4 illustrates the accuracy with which the modified Stafford-Smith and Carter equations represent the original curves.

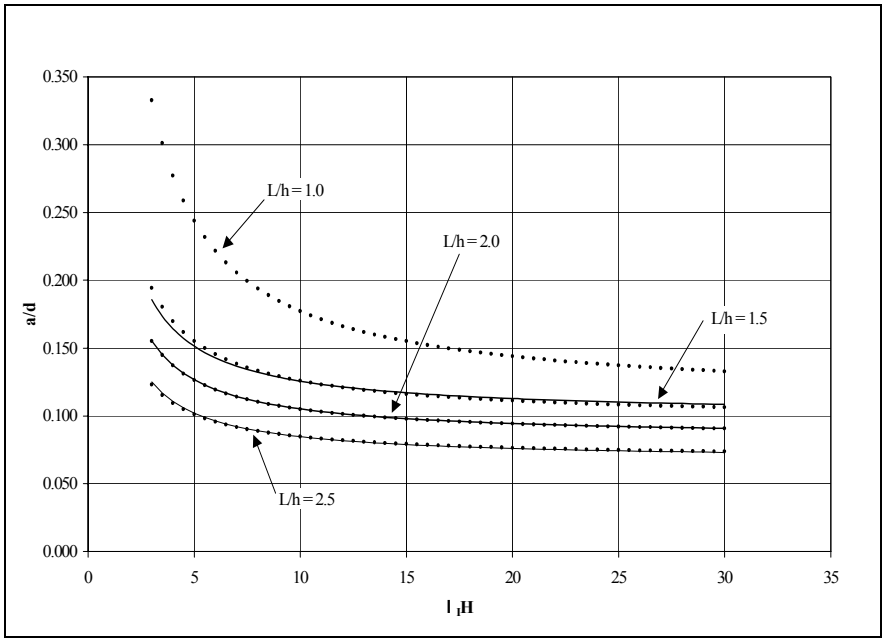

Figure B.4. Actual and modified SSC curves.

Original Stafford-Smith and Carter

$$a = 0.1106d\left(1 + \frac{6.027}{\lambda_1 H}\right) \quad for\ {}^{l}\!/_{h} = 1.0 \qquad \textbf{[Eq B.1]}$$

$$a = 0.0966d\left(1 + \frac{3.035}{\lambda_1 H}\right) \quad for\ {}^{l}\!/_{h} = 1.5 \qquad \textbf{[Eq B.2]}$$

$$a = 0.0835d\left(1 + \frac{2.574}{\lambda_1 H}\right) \quad for\ {}^{l}\!/_{h} = 2.0 \qquad \textbf{[Eq B.3]}$$

$$a = 0.0683d\left(1 + \frac{2.410}{\lambda_1 H}\right) \quad for\ {}^{l}\!/_{h} = 2.5 \qquad \textbf{[Eq B.4]}$$

Simplified Stafford-Smith and Carter

Equation 13

$$a = 0.0835Cd\left(1 + \frac{2.574}{\lambda_1 H}\right) \quad for\ {}^{l}\!/_{h} \geq 1.5$$

Equation 14

$$C = -0.3905\left(\frac{l}{h}\right) + 1.7829$$

Equation 15

$$a = 0.1106d\left(1 + \frac{6.027}{\lambda_1 H}\right) \quad for\ {}^{l}\!/_{h} = 1.0$$

A pushover analysis for a fully infilled 3x3 half-scale R/C frame, using the Mainstone (1971) equivalent strut width, overestimated the deflection at ultimate load by more than double that of the experimental value. Figure B.5 displays the base shear vs. deflection curves for both the pushover and experimental data.

The figure shows that, while the pushover analysis accurately predicted the ultimate base shear, it underestimated both the initial and post-yield stiffness values for the frame, with the initial portion being underestimated by nearly three times. This resulted in elevated displacements calculated at ultimate load.

Figure B.6 shows that, upon comparing the pushover and experimental load-deflection curves for the series of 1-story infilled frames, using the Mainstone (1971) equivalent strut width, a similar trend appeared. As the figure illustrates, the pushover analyses also overestimated displacements at ultimate load, though by only about 40 percent. This overestimation would have been more amplified, but the pushover analyses tended to underestimate ultimate capacity resulting in displacements at ultimate load that were smaller than would have otherwise been calculated. One significant similarity between the 3x3 model and the 1-story models was that the initial bilinear stiffness values for the 1-story models were also underestimated by about 300 percent on average. These stiffness values are shown in Table B.11.

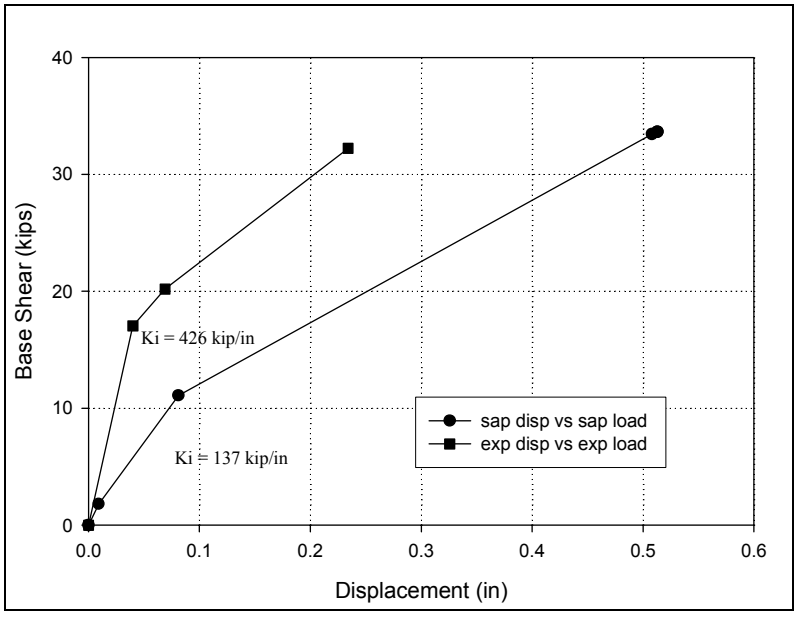

Figure B.5. Pushover vs. experimental for 3-bay 3-story masonry-infilled frames.

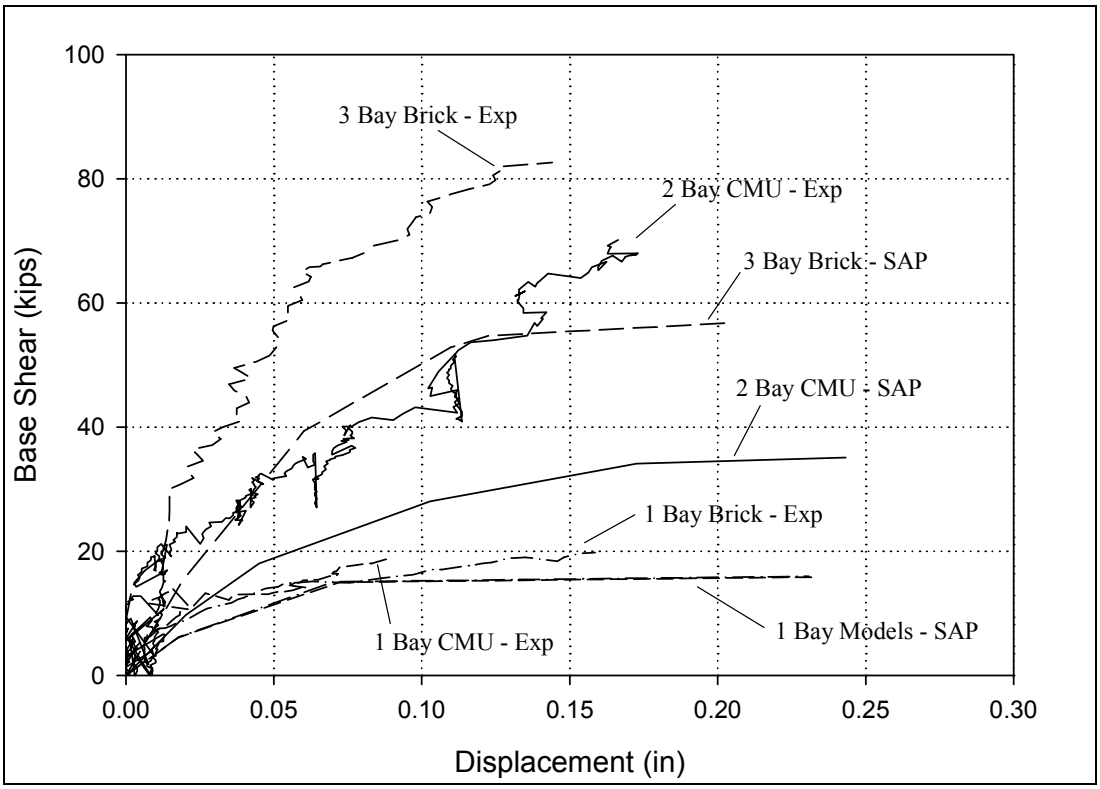

Figure B.6. Pushover vs. experimental for 1-story masonry-infilled frames.

Table B.11. Initial stiffness values.

Initial Experimental Stiffness	Initial Pushover Stiffness
3 Bay Brick - 2013 k/in.	3 Bay Brick - 633 k/in.
2 Bay CMU - 1366 k/in.	2 Bay CMU - 399 k/in.
1 Bay Models - 706 k/in.	1 Bay Models - 277 k/in.

To modify the pushover plots without unnecessary over-complication, the plots were estimated as being bilinear, as shown in Figures B.7 and B.8. Figure B.7 displays the original and bilinear pushover plots for each of the 1-story infilled R/C frames with their stiffness values listed in Table B.12. Figure B.8 shows a general case accompanied by the prescribed notation. As illustrated in Figure B.8, the initial portion of the bilinear curve is a simple straight line from the origin to a user-defined yield point (Δ_y, V_y). The post-yield bilinear portion of the curve is another straight line from the point of yielding to the point of ultimate load and deflection. The yield point was chosen to minimize the deviation (area between the plots) between the original pushover curve and its corresponding estimated bilinear curve.

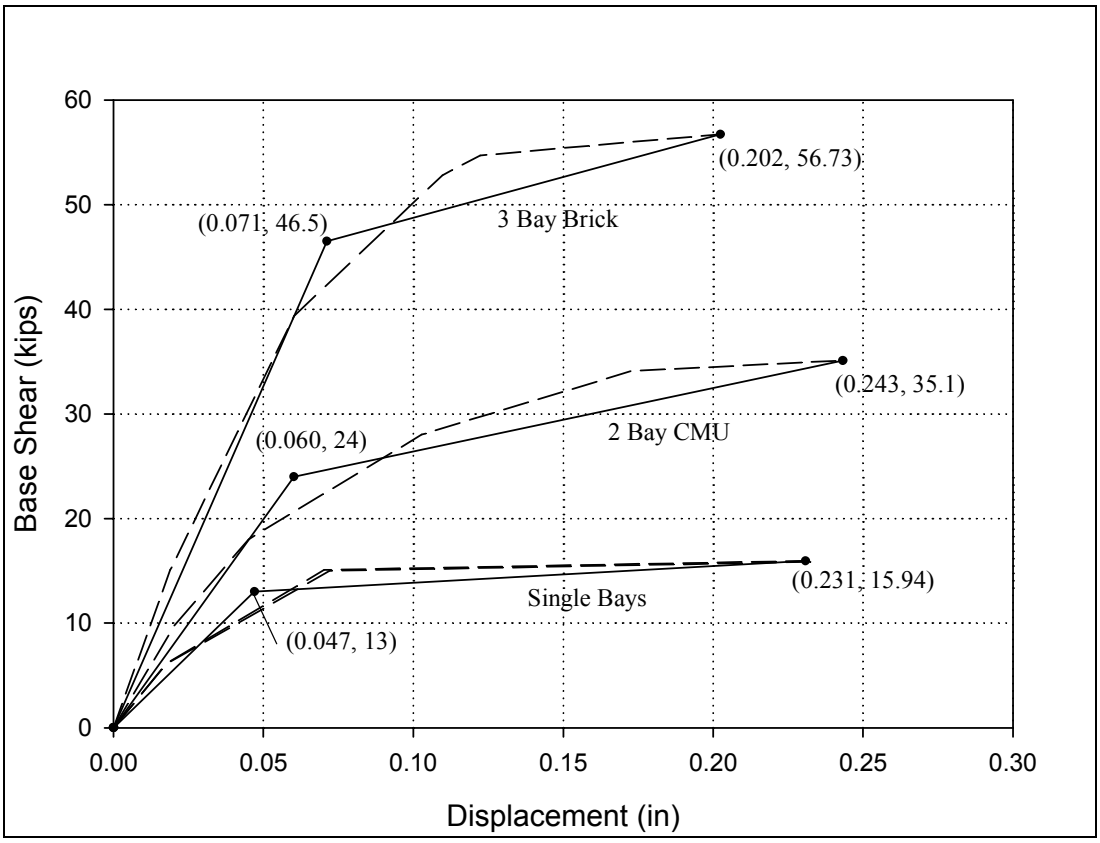

Figure B.7. Bilinear pushover plots.

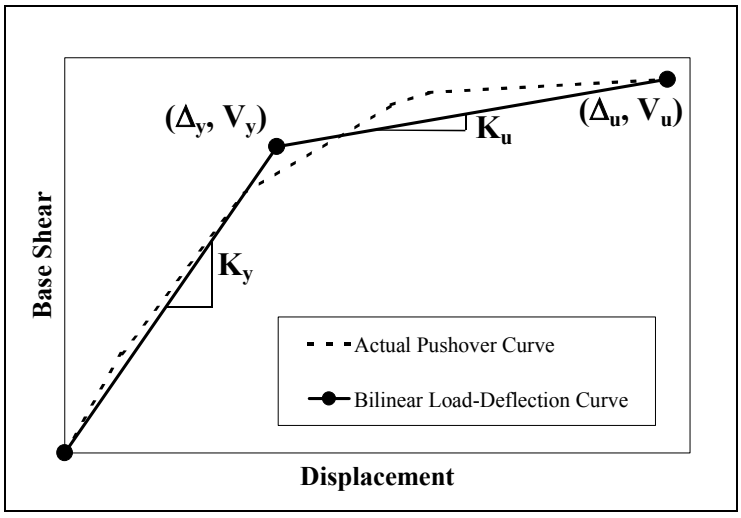

Figure B.8. General bilinear.

Table B.12. Bilinear stiffness values.

	K_1 (k/in.)	K_2 (k/in.)
3 Bay Brick	653	78
2 Bay CMU	399	61
1 Bay Models	277	16

A simple modification of these bilinear plots resulted in much improved ultimate displacement (Δ_u) estimations as well as very good estimates of initial stiffness. First, the previous yield (V_y) and ultimate (V_u) base shear values were maintained, then the initial bilinear stiffness (K_y) was multiplied by a factor of 3. This gives the actual initial stiffness (K_i), while post-yield bilinear stiffness (K_u) was multiplied by a factor of two to give a new slope (K_f) that yields reasonable values of displacement at ultimate load. Using these modified stiffness values, new plots were constructed. The initial bilinear portion of the plot with a slope of K_i was plotted up to the original yield point (V_y) as shown in Figure B.9. Then, the post-yield bilinear portion was plotted from the yield point up to the original ultimate base shear with a slope of K_f. Figure B.10 shows the resulting modified base shear vs. deflection curves for the 1-story half-scale models.

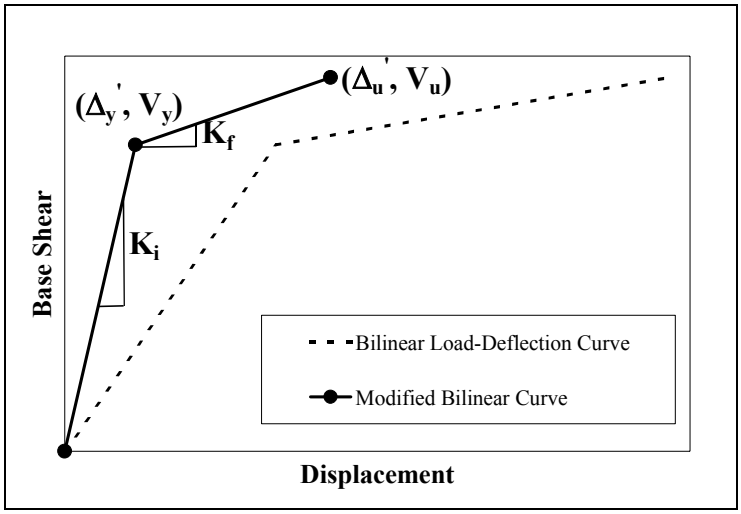

Figure B.9. General modifications.

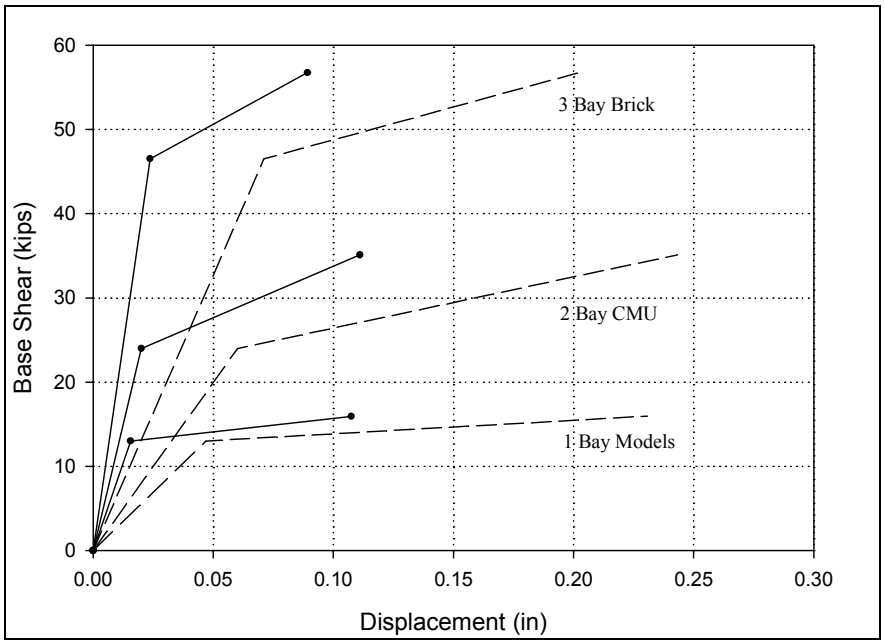

Figure B.10. Modified bilinear curves.

A comparison of the modified bilinear base shear vs. deflection curve and the experimental data plot for the half-scale 3x3 model is shown in Figure B.11. Figure B.12 comprises similar plots for the 1-story half-scale models. Figure B.11 clearly shows that the proposed method yielded an ultimate capacity, initial stiffness, and displacement at ultimate load that closely resemble those values found experimentally. For the 3x3 half-scale model, this method produced a value for initial stiffness that was within 3.5 percent of the experimental value while giving a displacement at ultimate that coincided with the experimental model within 4.3 percent. However, pushover analyses underestimated the ultimate base shear capacities of the 1-story half-scale models translating to low values for deflection at ultimate load. This resulted in initial stiffnesses that were within 12.6 percent on average, and displacements at ultimate that deviated by a little more than 30 percent on average. These deviations in ultimate capacity were already addressed in a previous section. Table B.13 summarizes the initial stiffnesses and displacements at ultimate load for the 3x3 and 1-story half-scale models.

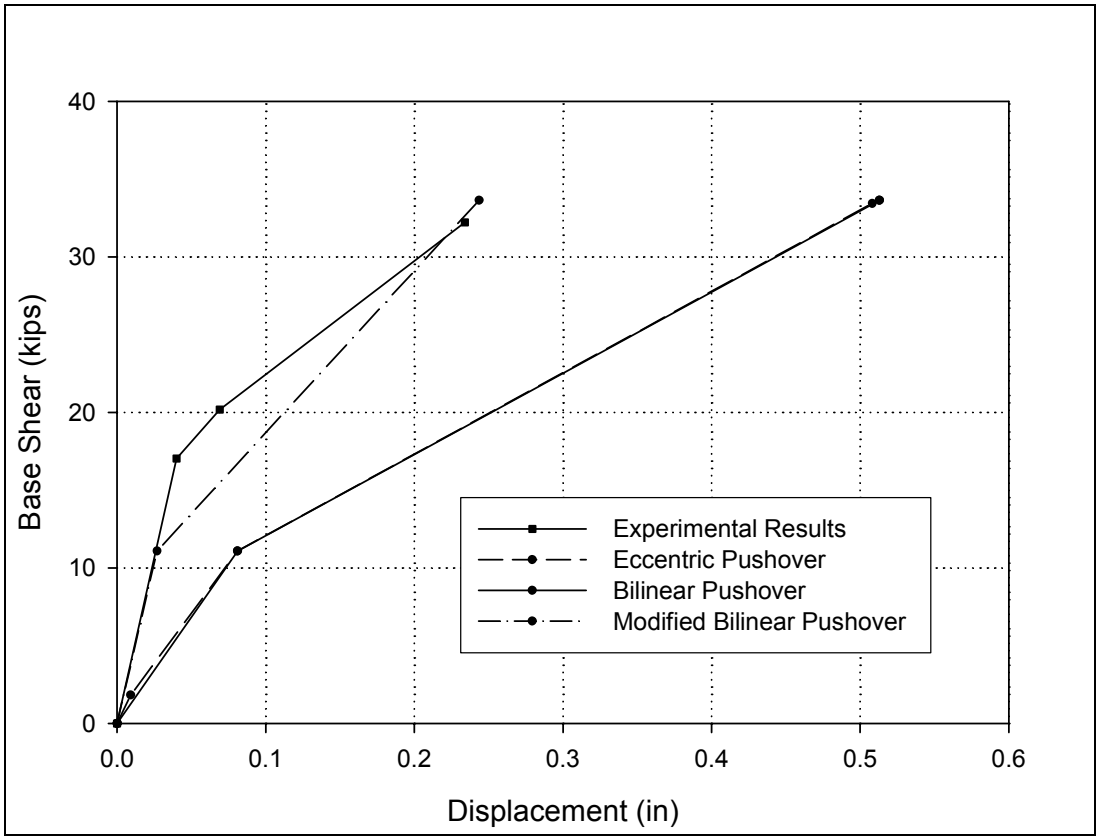

Figure B.11. Experimental vs. modified.

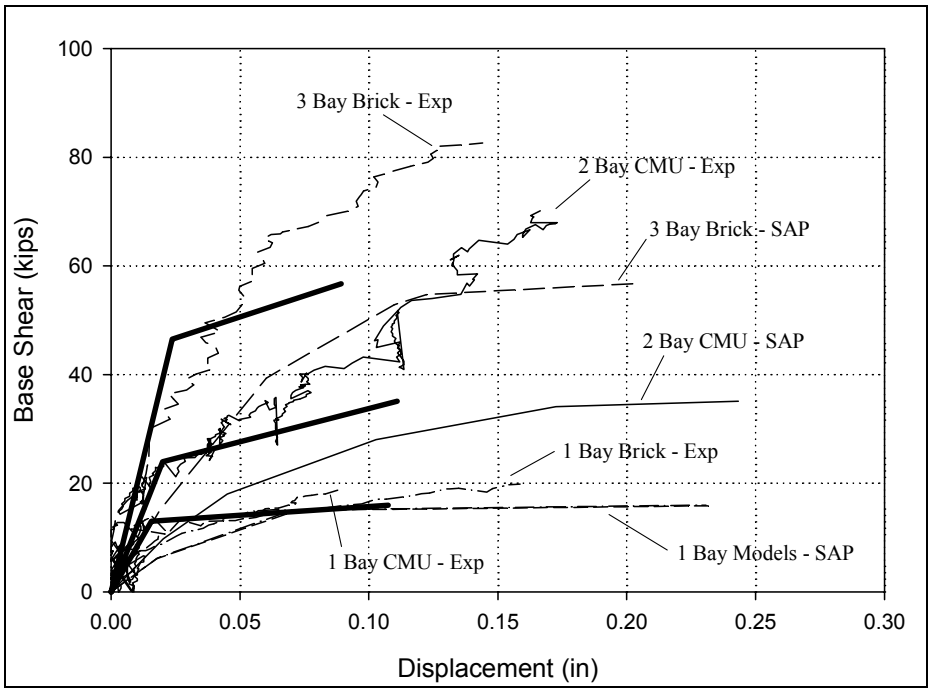

Figure B.12. Plot modification summary.

Table B.13. Stiffness and displacement values.

Model Description	Experimental Initial Stiffness (K/in)	Initial Bilinear Stiffness (K/in)	3 times Initial Bilinear Stiffness (K/in)	% Difference
3X3 fully-infilled	426	137	411	**-3.5**
1 Bay Brick	706	277	831	**17.7**
1 Bay CMU	706	277	831	**17.7**
2 Bay CMU	1366	399	1197	**-12.4**
3 Bay Brick	2013	653	1959	**-2.7**

Model Description	Experimental Displacement at Ultimate (in)	Displacement at Ultimate (in)	Modified Displacement (in)	% Difference
3X3 fully-infilled	0.234	0.513	0.244	**4.3**
1 Bay Brick	0.16	0.217	0.108	**-32.5**
1 Bay CMU	0.089	0.216	0.108	**21.3**
2 Bay CMU	0.166	0.21	0.111	**-33.1**
3 Bay Brick	0.144	0.19	0.089	**-38.2**

Alternatively, the Stafford-Smith and Carter (1969) equivalent strut equations can also be used to estimate the initial elastic stiffness for aspect ratios between 0.667 and 1.5, and must be implemented for any aspect ratios outside of this range. For the fully infilled half-scale model using Stafford-Smith and Carter (1969) equivalent struts, the initial elastic stiffness (K_{SSC}) matches the experimental data within 1.2 percent. Therefore, the initial stiffness as estimated by Stafford-Smith and Carter (1969) can also represent the value K_i. The expressions for estimated initial and post-yield bilinear stiffness can be written as Equations 16 and 17.

Note: The limitation on aspect ratio for using $3K_y$ for the initial stiffness was implemented since our FEA and experimental models were for l/h = 1.38.

Equation 16

$$K_i = \begin{cases} 3K_y & (0.67 \le \frac{l}{h} \le 1.5) \\ K_{SSC} & (any \quad \frac{l}{h}) \end{cases}$$

Equation 17

$$K_f = 2K_u$$

Next, it was necessary to correct the displacements given by FEA models with partial openings in order to verify the proposed stiffness modifications for structures with openings. To do so, two key assumptions were made. The modified displacements (3xK_1 and 2xK_2 as explained in Chapter 4) were assumed to be correct since this method predicted the displacement at ultimate load for a half-scale 3x3 fully infilled frame within 4.3 percent of the experimental value. Also, the full-scale models with partial door/window openings and DIP loading will produce a similar displacement ratio to the full-scale models with complete openings and CIP loading.

Experimental, FEA, and pushover displacement data were available for six different half-scale models. FEA for the five 1-story half-scale models yielded displacements that were, on average, 3.3 times less than those values found experimentally, as shown in Table B.14. When this factor was applied to the full-scale models with door/window openings and DIP loading, however, the resulting displacement values were still far too small, as shown in Table B.15. Furthermore, the trend in the FEA data suggested displacements at ultimate would increase if openings were introduced in the lower levels, while the pushover analyses predicted the opposite behavior. In addition, the FEA data for the 1-story half-scale models used to calculate the factor of 3.3 seemed suspiciously similar to one another. Not only were four of the five values almost identical in magnitude, but also all five values consisted of fours as the only non-zero digits (shown in Table B.15). Therefore, another means of correcting the FEA data for full-scale models with partial openings and DIP loading (original shear coefficient) needed to be found.

Table B.14. Displacement summary.

Opening Location	Nonlinear FEA (in)	Nonlinear FEA w/ 3.3 Correction	Modified Pushover (in)
---	0.028	0.094	0.345
3A	0.024	0.079	0.359
3B	0.027	0.090	0.359
2A	0.022	0.072	0.339
2B	0.048	0.158	0.324
1A	0.036	0.118	0.297
1B	0.034	0.111	0.287

Table B.15. Deflection summary.

Model Description	Nonlinear FEA Deflection (in)	Experimental Deflection (in)	Exp/FEA Ratio
1 Bay Brick	0.044	0.16	3.636
1 Bay CMU	0.04	0.089	2.225
2 Bay CMU	0.04	0.12	3.000
3 Bay Brick	0.044	0.148	3.364
1 Bay Bare	0.44	1.89	4.295
		Avg. Ratio	3.304

Table B.16 displays the FEA and pushover displacement trends for different types of openings, loading, and shear coefficient (FEA only). Note that all data, except FEA with the old shear coefficient, suggest that openings in the first floor will reduce displacement at ultimate, while openings in the third floor will increase displacements. This suggested outcome, coupled with the fact that the displacement trends for the models with complete openings agreed better with that of the pushover displacements, prompted the dismissal of the FEA displacements found with the old shear coefficient.

To generate displacement values at ultimate for models with partial openings, the assumption was made that the models with partial openings and DIP loading should have a displacement ratio similar to the models with complete openings and CIP loading. Furthermore, it was assumed that the pushover analyses predicted the displacement at ultimate for a fully infilled model accurately. By setting the displacement for the fully infilled FE model equal to the modified pushover displacement, and keeping the trend of the FEA data with the new shear coefficient and complete openings, a new set of displacements were created for FEA models with door/window openings. Therefore, a multiplication factor of 3.75 was applied to the FEA displacements in order to modify them to represent models with door/window openings. Comparing them to the modified pushover values translated into percent differences of 0 percent for fully infilled up to a maximum of 13.6 percent for openings in panel 2B (shown in Table B.17 with the percent differences highlighted in yellow).

Table B.16. Displacement trends.

Opening Location	Full-Scale Models with Complete Openings and CIP Loading (new shear coefficient)		Full-Scale Models with Partial Openings and DIP Loading (old shear coefficient)	
	Nonlinear FEA (in)	Pushover (in)	Nonlinear FEA (in)	Pushover (in)
---	0.092	0.770	0.028	0.755
3A	0.100	0.821	0.024	0.783
3B	0.102	0.824	0.027	0.793
2A	0.083	0.846	0.022	0.756
2B	0.100	0.871	0.048	0.719
1A	0.072	0.636	0.036	0.676
1B	0.063	0.654	0.034	0.662

Table B.17. Modification summary.

Opening Location	FEA Displacement at Ultimate for complete openings & CIP Loading (in) (new shear coeff.)	Modified* FEA Displacement at Ultimate for D/W Openings & DIP Loading (in)	Modified** Displacement at Ultimate (in)	% Difference
---	0.092	0.345	0.345	**0.0**
3A	0.1	0.375	0.359	**-4.3**
3B	0.102	0.383	0.359	**-6.1**
2A	0.083	0.311	0.339	**8.9**
2B	0.1	0.375	0.324	**-13.6**
1A	0.072	0.270	0.297	**10.0**
1B	0.063	0.304	0.287	**-5.5**

* FEA Displacements were modified to represent the displacement trends of FE models with the corrected shear retention value and also to agree with pushover results for the fully infilled model.

** Pushover Displacements were modified using 3xK1 and 2xK2 as explained in the first note*.

Out-of-Plane Strength Reduction for Infill Openings

To estimate the out-of-plane capacity of a partially infilled frame, it is necessary to apply a reduction factor to account for openings in the infill panel. With no experimental data to compare with, the decision was made that a linear relationship between the size of the opening and the size of the infill panel would be the most reasonable assumption. The next detail to consider was whether or not a ratio of opening size/panel size based on perimeter or area would better represent the reduction in out-of-plane strength. Reduction factors were therefore calculated for both perimeter and area ratios according to Figure B.13 using various opening configurations and panel aspect ratios.

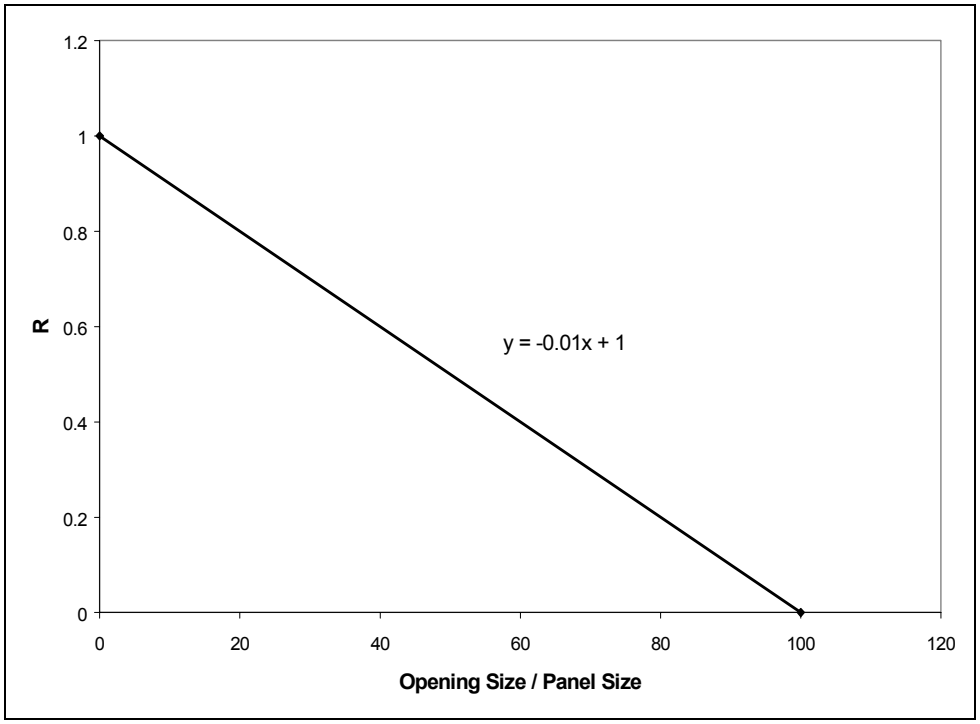

Figure B.13. Reduction factor vs. ratio.

After calculation, it was noticed that, for the perimeter ratio, rather large reduction factors were calculated for relatively small openings while the opposite was not true for larger openings. Conversely, the reduction factors calculated from the area ratio varied much more linearly with respect to the relative size of the opening. Tables B.18 and B.19 show the reduction factors calculated using both area and perimeter ratios as well as for the in-plane case (which coincided with experimental data). Table B.18 represents a 12-ft by 12-ft frame (aspect ratio = 1.0) for various opening configurations while Table B.19 represents a 12-ft by 6-ft frame (aspect ratio = 0.5).

Table B.18. Reduction factors (1/h = 1.0).

lopen	hopen	Aopen	Popen	Aopen / Apanel	Popen / Ppanel	R(Area)	R(perimeter)	R(in-plane)
0	0	0	0	0.0	0.0	1.000	1.000	1.000
2	2	4	8	2.8	16.7	0.972	0.833	0.956
2	4	8	12	5.6	25.0	0.944	0.750	0.913
2	6	12	16	8.3	33.3	0.917	0.667	0.871
2	8	16	20	11.1	41.7	0.889	0.583	0.830
2	10	20	24	13.9	50.0	0.861	0.500	0.789
2	12	24	28	16.7	58.3	0.833	0.417	0.750
4	4	16	16	11.1	33.3	0.889	0.667	0.830
4	6	24	20	16.7	41.7	0.833	0.583	0.750
4	8	32	24	22.2	50.0	0.778	0.500	0.674
4	10	40	28	27.8	58.3	0.722	0.417	0.602
4	12	48	32	33.3	66.7	0.667	0.333	0.533
6	6	36	24	25.0	50.0	0.750	0.500	0.638
6	8	48	28	33.3	58.3	0.667	0.417	0.533
6	10	60	32	41.7	66.7	0.583	0.333	0.438
6	12	72	36	50.0	75.0	0.500	0.250	0.350
8	8	64	32	44.4	66.7	0.556	0.333	0.407
8	10	80	36	55.6	75.0	0.444	0.250	0.296
8	12	96	40	66.7	83.3	0.333	0.167	0.200
10	10	100	40	69.4	83.3	0.306	0.167	0.178
10	12	120	44	83.3	91.7	0.167	0.083	0.083
12	12	144	48	100.0	100.0	0.000	0.000	0.000

Table B.19. Reduction factors (1/h = 0.5).

lopen	hopen	Aopen	Popen	Aopen / Apanel	Popen / Ppanel	R(Area)	R(perimeter)	R(in-plane)
0	0	0	0	0.0	0.0	1.000	1.000	1.000
2	2	4	8	5.6	22.2	0.944	0.778	0.913
2	4	8	12	11.1	33.3	0.889	0.667	0.830
2	6	12	16	16.7	44.4	0.833	0.556	0.750
2	8	16	20	22.2	55.6	0.778	0.444	0.674
2	10	20	24	27.8	66.7	0.722	0.333	0.602
2	12	24	28	33.3	77.8	0.667	0.222	0.533
4	4	16	16	22.2	44.4	0.778	0.556	0.674
4	6	24	20	33.3	55.6	0.667	0.444	0.533
4	8	32	24	44.4	66.7	0.556	0.333	0.407
4	10	40	28	55.6	77.8	0.444	0.222	0.296
4	12	48	32	66.7	88.9	0.333	0.111	0.200
6	6	36	24	50.0	66.7	0.500	0.333	0.350
6	8	48	28	66.7	77.8	0.333	0.222	0.200
6	10	60	32	83.3	88.9	0.167	0.111	0.083
6	12	72	36	100.0	100.0	0.000	0.000	0.000

(Note: The reduction factor for in-plane evaluation was plotted for comparison, but was not necessarily used as a basis since it represents in-plane strength, while the goal of this section was to determine the out-of-plane reduction.)

As Table B.19 indicates, the perimeter ratio reduces strength too much for the relatively small openings. The 2-ft by 2-ft opening (the smallest opening configuration examined), for example, had an average reduction on the order of 20 percent for the perimeter ratio while the area ratio and in-plane reduction were both within 5 percent of one another. For this reason, the area ratio was chosen as the preferred reduction for infill openings evaluated for out-of-plane capacity.

Rather than simply use a straight linear variation, however, it was decided that no strength reduction should result for openings less than or equal to 20 percent of the panel area. This resulted in the strength reduction factor $(R_1)_o$ calculated from Equation 19, represented graphically in Figure B.14.

Equation 19

$$(R_1)_o = \frac{5}{4}\left(1 - \frac{A_{open}}{A_{panel}}\right)$$

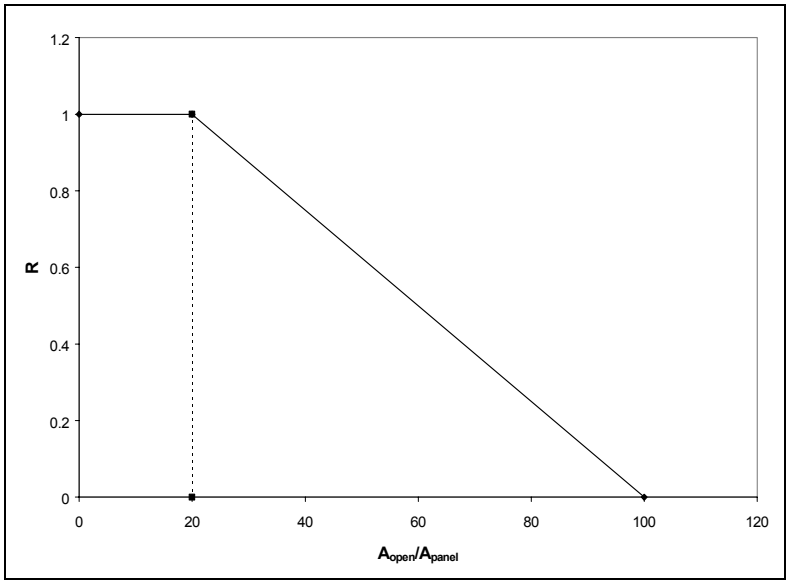

Figure B.14. Representation of Equation 19.

Effect of Out-of-Plane Loading on In-Plane Capacity

The reduction factor for perforated panels, combined with a slenderness parameter λ_o (Table 3), a reduction for existing infill damage $(R_2)_o$ (Table 4), and a reduction for flexibility of frame elements $(R_3)_o$ (Equation 20) are inserted in Equation 18 to estimate the frame's out-of-plane capacity. Upon calculation of the out-of-plane capacity and the in-plane capacity explained in Chapter 3, it is useful to determine a method for estimating an in-plane capacity reduction based on an out-of-plane demand.

To determine a suitable relationship, the ratio of $IP_{reduced}/IP_{ultimate}$ was plotted against $OP_{demand}/OP_{capacity}$. Nonlinear finite element results were plotted in this fashion for two 1-bay, 1-story frames, one infilled with brick masonry and the other with CMU. Table B.20 shows these load and capacity values along with their corresponding ratios, while the resulting plot is depicted in Figure B.15.

Due to the definitions of the plotted ratios, neither should exceed unity in the equation. In addition, it was assumed that small OP demands would not affect IP capacity and could be ignored. It should be assumed, therefore, that there is no reduction for in-plane capacity if the out-of-plane demand is less than or equal to 20 percent of the out-of-plane capacity. This effect is depicted in the revised chart located in Figure B.16, with Equation 21 showing the numerical interpretation for the reduction of in-plane capacity due to out-of-plane demand.

Table B.20. Capacity/demand values.

1-Bay CMU			
Out-of-Plane (kN)	**In-Plane (kN)**	R_{OP}	R_{IP}
38.6	0	1	0
19.3	416	0.5	0.8353
0	498	0	1

1-Bay Brick			
Out-of-Plane *(kN)*	**In-Plane** *(kN)*	R_{OP}	R_{IP}
57.4	0	1	0
28.7	418	0.5	0.7901
0	529	0	1
(Note: R_{OP} is defined as $OP_{demand}/OP_{capacity}$)			
(Note: R_{IP} is defined as $IP_{reduced}/IP_{ultimate}$)			

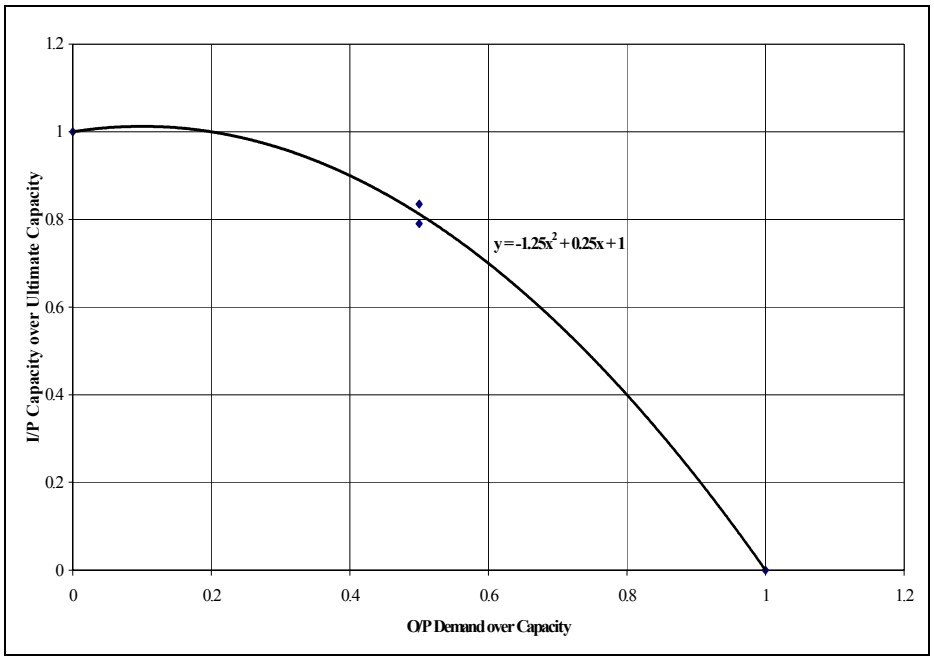

Figure B.15. Effect of OP on IP capacity.

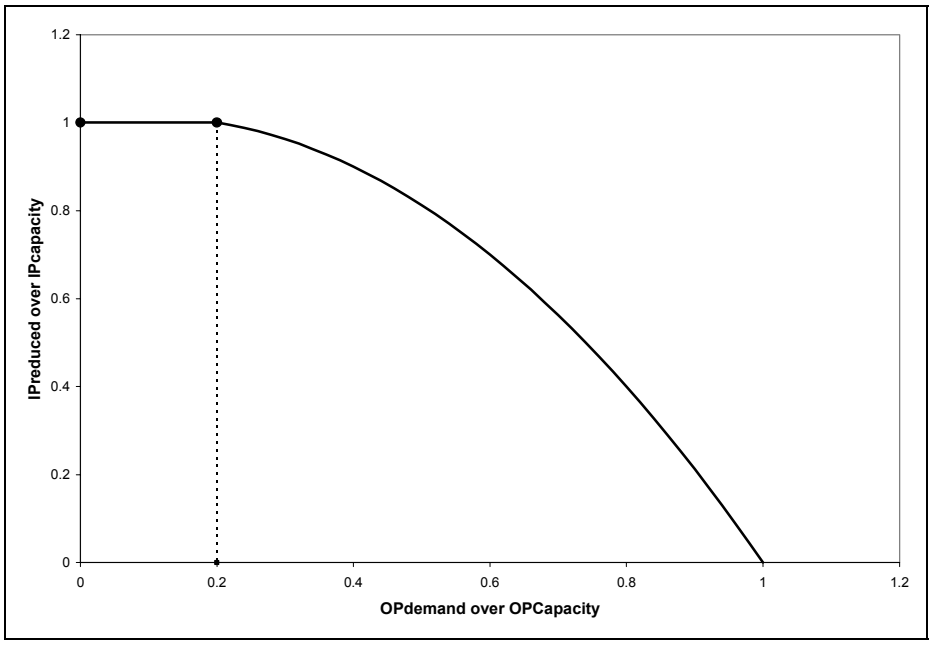

Figure B.16. Effect of OP on IP revised.

Equation 21

$$\frac{IP_{reduced}}{IP_{capacity}} = 1 + \frac{1}{4}\frac{OP_{demand}}{OP_{capacity}} - \frac{5}{4}\left(\frac{OP_{demand}}{OP_{capacity}}\right)^2$$

Alternative Methods of Analysis

A linear analysis of the infilled frame was performed using the example structure presented in Appendix A. The ultimate base shear for this frame (152 kips), found from the pushover analysis executed in Appendix A, was applied to the linear model with the same vertical triangular distribution. Demand over capacity ratios were computed for all members. Table B.21 lists axial, shear, moment, and axial-flexure demand for all members. The highest demand to capacity ratio was 1.73 from beam 1C. This value infers that a linear analysis of this frame, limiting all demand to capacity ratios to unity, would have underestimated the ultimate capacity by 73 percent. Using this value as a basis, a conservative increase in strength of 50 percent is recommended if one chooses to perform a linear analysis rather than a pushover analysis.

Table B.21. Demand over capacity values for the linear analysis of the example structure.

STRUTS

	Axial Force (K)		
Member	Demand	Capacity	D/C
3C	16.57	77.8	0.21
3B	19.33	77.8	0.25
3A	15.53	77.8	0.20
2C	27.76	77.8	0.36
2B	31.04	77.8	0.40
2A	27.28	77.8	0.35
1C	9.46	44.1	0.21
1B	33.75	77.8	0.43
1A	34.16	77.8	0.44

BEAMS

	Positive Moment (K-in)		
Member	Demand	Capacity	D/C
3C	414.53	702	0.59
3B	351.73	702	0.50
3A	234.12	702	0.33
2C	896.77	702	**1.28**
2B	819.54	702	**1.17**
2A	735.94	702	**1.05**
1C	1215.99	702	**1.73**
1B	1085.47	702	**1.55**
1A	1167.39	702	**1.66**

	Negative Moment (K-in)		
Member	Demand	Capacity	D/C
3C	314.85	1171	0.27
3B	362.53	1171	0.31
3A	280.6	1171	0.24
2C	795.13	1171	0.68
2B	829.31	1171	0.71
2A	799.19	1171	0.68
1C	1120.17	1171	0.96
1B	1083.93	1171	0.93
1A	1324.42	1171	**1.13**

	Shear (K)		
Member	Demand	Capacity	D/C
3C	6.63	28.61	0.23
3B	6.49	28.61	0.23
3A	4.68	28.61	0.16
2C	15.38	28.61	0.54
2B	14.99	28.61	0.52
2A	13.96	28.61	0.49
1C	21.24	28.61	0.74
1B	19.72	28.61	0.69
1A	22.65	28.61	0.79

COLUMNS

	P (K)	Mmax (K-in)	Moment	
Member	Demand	Demand	Capacity	D/C
3D	-14.19	217.48	719	0.30
3C	-8.68	468.58	719	0.65
3B	-5.27	432	719	0.60
3A	4.68	286.46	719	0.40
2D	-42.23	409.3	719	0.57
2C	-14.89	675.03	719	0.94
2B	-7.86	668.53	719	0.93
2A	25.72	414.11	719	0.58
1D	-67.79	926.66	719	**1.29**
1C	-16.1	1019.98	719	**1.42**
1B	-12.21	1030.5	719	**1.43**
1A	60.81	895.49	719	**1.25**

	Shear (K)		
Member	Demand	Capacity	D/C
3D	4.35	31.22	0.14
3C	10.49	31.22	0.34
3B	9.55	31.22	0.31
3A	5.85	31.22	0.19
2D	9.53	31.22	0.31
2C	15.95	31.22	0.51
2B	15.79	31.22	0.51
2A	8.79	31.22	0.28
1D	19.42	31.22	0.62
1C	22.51	31.22	0.72
1B	22.89	31.22	0.73
1A	18.32	31.22	0.59

Glossary

Definitions

Axial Hinge: A plastic hinge defined to model the inelastic action of a structural member when its yield strength is surpassed due to axial forces.

Axial-Moment Hinge: A plastic hinge defined to model the inelastic action of a structural member when its yield strength is surpassed due to the combination of axial loads and bending moments.

Building Type: A building classification, shown in Table 1, defined by FEMA 310, that groups together building types with common lateral force resisting systems.

Existing Infill Damage: Damage experienced by the infill during its service life.

Frame: A structural system of beams and columns that resists vertical/lateral loads.

Infill Aspect Ratio: Ratio of full length to height dimensions for masonry infill panels (l/h).

Infill Slenderness Ratio: Ratio of full height to thickness dimensions for masonry infill panels (h/t).

Infill Strength: The maximum lateral loads that a masonry infill panel can resist (psf).

Infilled Frame: Lateral and vertical load resisting structural systems that consist of frame and infill panels. The infill can be full, partial, or contain openings.

Isolated Masonry Infill Panel: A specific type of masonry infill panel in which the panel and the confining frame are in direct contact at the panel base only. The other three panel sides are not in contact with the frame.

Life Safety Performance Level: Building performance that includes significant damage to both structural and nonstructural components during an earthquake, though at least some margin against either partial or total structural collapse remains. Injuries may occur, but entrapment is low.

Masonry Infill Panel: A masonry wall constructed within an existing confining frame. These panels are built in-place and should be constructed so that there is full contact along the entire perimeter of the infill.

Moment Hinge: A plastic hinge defined to model the inelastic action of a structural member when its yield strength is surpassed due to bending moment forces.

Mortar Joint: A mixture of sand, cement, lime, and water that is used to bond masonry units together.

Plastic Hinge: Location of inelastic action on a structural member.

Rigid End Offset: The length of a structural member assumed to be completely rigid in order to model the effects of full contact between the infill and structural members.

Shear Hinge: A plastic hinge defined to model the inelastic action of a structural member when its yield strength is surpassed due to shear forces.

Solid Infill Panel: A masonry infill panel built with solid masonry units (such as clay brick).

Ultimate Load: The maximum value of base shear predicted by a nonlinear structural pushover analysis.

Yield Load: Value of base shear on a bilinear estimate of a pushover curve at which the slope changes and the model becomes more flexible.

Symbols

a	Equivalent width of infill strut in the elastic range (in.)
A_g	Gross cross sectional area of confining frame elements (in.^{2})

A_n Net cross sectional mortar/grouted area of infill panel along its length (in.^{2})

A_{open} Total area of openings in a selected infill panel (in.^{2})

A_{panel} Gross area of an infill panel (in.^{2})

A_s Steel cross sectional area in the concrete members (in.^{2})

b_b Width of a confining frame beam element (in.)

b_c Width of a confining frame column element (in.)

C A multiplication factor for calculating strut width that accounts for aspect ratio

d Nonlinear drift associated with the infill panel (%)

D Diagonal length of infill (in.)

E_c Modulus of elasticity of confining frame (psi)

E_m Modulus of elasticity of masonry in compression (psi)

E_s Modulus of elasticity of the steel (psi)

f'_c Compressive strength of concrete (psi)

f'_m Compressive strength of masonry (psi)

f'_t Masonry flexural tensile strength (psi)

f'_v Masonry shear strength (psi)

f_y Yield strength of the steel (psi)

G_m Masonry shear modulus ($0.4\ E_m$) (psi)

H Height of the confining frame (in.)

h Height of the infill panel (in.)

h/t Infill panel slenderness ratio

h_b Height of a confining frame beam element (in.)

h_c Height of a confining frame column element (in.)

$h_{opening}$ Height of individual infill opening (in.)

I_{beam} Moment of inertia of confining beam (in.^{4})

I_{column} Moment of inertia of confining column (in.^{4})

I_{frame} Lesser Moment of inertia between I_{beam} and I_{column} (in.^{4})

$IP_{capacity}$ Ultimate in-plane loading capacity (kips)

$IP_{reduced}$ Reduced in-plane loading capacity resulting from out-of-plane forces (kips)

K_i Modified initial bilinear stiffness (k/in.)

K_f Modified post-yield bilinear stiffness (k/in.)

K_{SSC} Initial bilinear stiffness as estimated from Stafford-Smith and Carter (1969) (k/in.)

K_y Initial bilinear stiffness as estimated from Mainstone (1971) (k/in.)

K_u Post-yield bilinear stiffness as estimated from Mainstone (1971) (k/in.)

l Length of the infill panel (in.)

l/h Infill panel aspect ratio

l_{beam} Distance from the face of the beam to the first beam plastic hinge (in.)

l_{column} Distance from the face of the column to the first column plastic hinge (in.)

L_f Length of the confining frame (in.)

$L_{opening}$ Length of individual infill opening (in.)

OP_{demand} Out-of-plane load that a structure is required to withstand (kips)

$OP_{capacity}$ Out-of-plane load that a structure is capable of withstanding (kips)

R_{cr} Force required to reach the masonry infill panel's crushing strength (lb)

R_{shear} Force required to reach the masonry infill panel's shear strength (lb)

R_{strut} minimum of R_{cr} and R_{shear} (lb)

$(R_1)_i$ In-plane reduction factor that accounts for the presence of infill openings

$(R_1)_o$ Out-of-plane reduction factor that accounts for the presence of infill openings

$(R_2)_i$ In-plane reduction factor that accounts for existing panel damage

$(R_2)_o$ Out-of-plane reduction factor that accounts for existing panel damage

$(R_3)_o$ Out-of-plane reduction factor that accounts for the flexibility of the confining frame

t Gross thickness of the infill (in.)

t_{eff} Effective net thickness of the infill (in.)

V_y Estimated bilinear "yield" strength of a structure (kips)

V_u Ultimate capacity of a structure as computed by a pushover analysis (kips)

w Parameter used in the out-of-plane strength evaluation of masonry infill panels (psi)

δ Out-of-Plane infill deflection at the center (mid-height) of the panel (in.)

Δ In-Plane lateral deformation experienced by the structure (in.)

Δ_u Bilinear deflection at ultimate load as computed by a pushover analysis (in.)

Δ_y Estimated bilinear "yield" deflection (in.)

Δ_u' Modified bilinear deflection at ultimate load (in.)

Δ_y' Modified bilinear "yield" deflection (in.)

ε_{cr} Ultimate crushing strain of masonry (in./in.)

λ_o Parameter required to evaluate the out-of-plane infill strength

λ_I Relative infill to frame stiffness parameter

θ Angle of the concentric equivalent strut (degrees)

θ_{beam} Angle between face of the eccentric equivalent strut and the horizontal if the strut were to be modeled eccentrically along the beam (degrees)

θ_{column} Angle between face of the eccentric equivalent strut and the horizontal if the strut were to be modeled eccentrically along the column (degrees)

θ_{strut} Angle made between the eccentric equivalent strut and the horizontal if the strut is modeled as a center-line element (degrees)

CERL Distribution

Chief of Engineers
ATTN: CEHEC-IM-LH (2)
ATTN: CECW-EW

Engineer Research and Development Center (Libraries)
ATTN: ERDC, Vicksburg, MS
ATTN: Cold Regions Research, Hanover, NH
ATTN: Topographic Engineering Center, Alexandria, VA

Defense Tech Info Center 22304
ATTN: DTIC-O

10
12/01

REPORT DOCUMENTATION PAGE

Form Approved
OMB No. 0704-0188

1. REPORT DATE (DD-MM-YYYY)	2. REPORT TYPE	3. DATES COVERED (From - To)
01-2002	Final	

4. TITLE AND SUBTITLE
Evaluating Strength and Stiffness of Unreinforced Masonry Infill Structures

5a. CONTRACT NUMBER

5b. GRANT NUMBER

5c. PROGRAM ELEMENT NUMBER

6. AUTHOR(S)
Ghassan Al-Chaar

5d. PROJECT NUMBER
622784AT41

5e. TASK NUMBER

5f. WORK UNIT NUMBER
CFM-A011

7. PERFORMING ORGANIZATION NAME(S) AND ADDRESS(ES)
U.S. Army Engineer Research and Development Center (ERDC)
Construction Engineering Research Laboratory (CERL)
P.O. Box 9005
Champaign, IL 61826-9005

8. PERFORMING ORGANIZATION REPORT NUMBER
ERDC/CERL TR-02-1

9. SPONSORING / MONITORING AGENCY NAME(S) AND ADDRESS(ES)
Headquarters, U.S. Army Corps of Engineers
441 G Street, NW
Washington, DC 20314-1000

10. SPONSOR/MONITOR'S ACRONYM(S)
CECW-E

11. SPONSOR/MONITOR'S REPORT NUMBER(S)

12. DISTRIBUTION / AVAILABILITY STATEMENT
Approved for public release; distribution is unlimited.

13. SUPPLEMENTARY NOTES
Copies are available from the National Technical Information Service, 5285 Port Royal Road, Springfield, VA 22161.

14. ABSTRACT

Masonry has been used for hundreds of years around the world in construction projects ranging from simple roadways to complex arch designs. Masonry is also commonly used in frame building structures as infill to either protect the inside of the structure from the environment or to divide inside spaces. During the design and analysis of steel/reinforced concrete frame structures, infill has commonly been ignored. Contrary to common practice, masonry infills do influence the overall behavior of structures when subjected to lateral forces. The influence of infills on overall behavior of the structure has been found to change with the direction in which the load is applied.

This report gives guidelines on evaluating the lateral load capacity of infilled panels for in-plane and out-of-plane loading. Further guidelines account for the effect of out-of-plane loading on in-plane capacity. This report is a complement to applicable provisions in FEMA 310 with respect to seismic evaluation of buildings. These guidelines should prove useful for engineering evaluations of the lateral strength of buildings with respect to wind or earthquake forces. The guidelines give the engineer a strength-based alternative to FEMA 273, a performance-based method, which should also result in safe and economical construction.

15. SUBJECT TERMS

masonry	unreinforced masonry (URM)	lateral force
structural engineering	infill panels	seismic testing

16. SECURITY CLASSIFICATION OF:			17. LIMITATION OF ABSTRACT	18. NUMBER OF PAGES	19a. NAME OF RESPONSIBLE PERSON
a. REPORT	b. ABSTRACT	c. THIS PAGE			Dr. Ghassan Al-Chaar
Unclassified	Unclassified	Unclassified	SAR	88	19b. TELEPHONE NUMBER (include area code) (217)373-7247